



Autophagy–mediated plasma membrane removal promotes the formation of epithelial syncytia

Parisa Kakanj^{1,2,3,4,*} , Sourabh Bhide^{2,5}, Bernard Moussian⁶ & Maria Leptin^{1,2,3,4,**} 

Abstract

Epithelial wound healing in *Drosophila* involves the formation of multinucleate cells surrounding the wound. We show that autophagy, a cellular degradation process often deployed in stress responses, is required for the formation of a multinucleated syncytium during wound healing, and that autophagosomes that appear near the wound edge acquire plasma membrane markers. In addition, uncontrolled autophagy in the unwounded epidermis leads to the degradation of endo-membranes and the lateral plasma membrane, while apical and basal membranes and epithelial barrier function remain intact. Proper functioning of TORC1 is needed to prevent destruction of the larval epidermis by autophagy, in a process that depends on phagophore initiation and expansion but does not require autophagosomes fusion with lysosomes. Autophagy induction can also affect other sub-cellular membranes, as shown by its suppression of experimentally induced laminopathy-like nuclear defects. Our findings reveal a function for TORC1-mediated regulation of autophagy in maintaining membrane integrity and homeostasis in the epidermis and during wound healing.

Keywords cell junction; gut barrier; myosin; nuclear morphology; wound healing

Subject Categories Autophagy & Cell Death; Cell Adhesion, Polarity & Cytoskeleton

DOI 10.15252/emboj.2021109992 | Received 19 October 2021 | Revised 8 February 2022 | Accepted 10 February 2022 | Published online 9 March 2022

The EMBO Journal (2022) 41: e109992

See also: R Khezri & TE Rusten (June 2022)

Introduction

Autophagy is a conserved intracellular degradation process that engulfs cytoplasmic materials in double membrane vesicles, the autophagosomes, and delivers them to lysosomes (Allen & Baehrecke, 2020). Multiple organelles, such as the endoplasmic reticulum (ER), Golgi, mitochondria, nuclear envelope and plasma

membrane, can provide membrane to form pre-autophagosomal structures (PAS) and nucleate phagophores (Ravikumar *et al.*, 2010; Pavel & Rubinsztein, 2017). Autophagy occurs during development, differentiation and tissue remodelling, and it can be activated in response to intracellular or extracellular stresses such as DNA damage, protein aggregates, damaged organelles, starvation, heat shock, oxidative stress infection or wounding (Levine & Kroemer, 2019; Sylakowski & Wells, 2021).

Wounding has been shown in *Drosophila*, planarians, zebrafish, rat, mouse and plants to induce autophagy (Varga *et al.*, 2014; Kakanj *et al.*, 2016; Kang *et al.*, 2019; Allen & Baehrecke, 2020; Chavez *et al.*, 2020; Kurotani *et al.*, 2020; Qiang *et al.*, 2020; Xu *et al.*, 2020). In plants, rats and mice, autophagy is in turn necessary for efficient wound healing. Plant grafting induces autophagy at the site of the wound and lack of Atg2 or Atg5 reduces the rate of successful grafting (Kurotani *et al.*, 2020). Wounding mouse skin induces the expression of autophagy genes in the epidermis and some of these genes (Atg5 or Atg7) are needed for proper wound closure, infiltration by immune cells, and for the production of cytokine CCL2. Applying recombinant CCL2 can reverse the effect of impaired autophagy indicating that the main role of autophagy in this context is to promote wound healing by inducing the production of CCL2 (Qiang *et al.*, 2020). In rats, elevated autophagy at the wound margin is required for clearance of bacteria. Both autophagy and bacterial clearance are reduced in diabetic rats, but can be ameliorated by inhibiting TOR signalling with rapamycin (Xu *et al.*, 2020). These findings illustrate a role for autophagy in wound healing, but many of the molecular mechanisms involved are unclear. Here, we used *Drosophila* larvae to investigate the cellular function and physiological role of autophagy in the epidermis and during wound healing.

The epidermis of *Drosophila* larva is a monolayer of polyploid, postmitotic epithelial cells on a basal lamina, attached on its apical side to the cuticle (Galko & Krasnow, 2004; Gangishetti *et al.*, 2012). Larval wound healing is driven by two parallel and coordinated mechanisms. Actomyosin assembly and contraction at the apical side and lamellipodia on the basal side of the cells surrounding the wound lead to elongation of these cells into the wound to close the gap (Galko & Krasnow, 2004; Kakanj *et al.*, 2016). Autophagy occurs

1 Institute for Genetics, University of Cologne, Cologne, Germany

2 Director's Research Unit, European Molecular Biology Laboratory, Heidelberg, Germany

3 Center for Molecular Medicine Cologne, University of Cologne, Cologne, Germany

4 Cologne Excellence Cluster on Cellular Stress Responses in Aging-Associated Diseases, University of Cologne, Cologne, Germany

5 Faculty of Biosciences, Collaboration for Joint PhD degree between EMBL and Heidelberg University, Heidelberg, Germany

6 Université Côte d'Azur, Parc Valrose, Nice, France

*Corresponding author. Tel: +49 221 4703528; E-mail: pkakanj@uni-koeln.de

**Corresponding author. Tel: +49 221 4703401; E-mail: mleptin@uni-koeln.de

in cells surrounding the wound as they close the wound (Kakanj *et al*, 2016). Another late event in wound healing in larvae, pupa and adult flies is the formation of a multinucleate syncytium (Galko & Krasnow, 2004; Losick *et al*, 2013; Wang *et al*, 2015).

One of the pathways activated during wound healing is the JNK pathway. Hyperactivation of JNK leads to disassembly of focal adhesion complexes and induces syncytium formation in unwounded epidermis (Galko & Krasnow, 2004; Wang *et al*, 2015). However, the natural syncytium formation in cells surrounding wounds does not depend on JNK signalling (Wang *et al*, 2015). This suggests that parallel to JNK other signals are involved in syncytium formation after wounding.

In the adult fly, syncytium formation during wound healing involves polyploidization and cell fusion, both dependent on Hippo/Yorkie signalling (Losick *et al*, 2013; Besen-McNally *et al*, 2021). While no connection with autophagy was shown in this system, it is worth noting that Yorkie can activate TORC1, a direct suppressor of autophagy, and that TORC1 is activated during larval wound healing, where it supports wound closure partly through S6K, one of its downstream effectors (Kakanj *et al*, 2016; Wang *et al*, 2020).

Whether autophagy and syncytium formation are causally connected is not known. However, during ageing a progressive elevation of autophagy drives epidermal remodelling, morphological deterioration and formation of large multinuclear cells (Scherfer *et al*, 2013). Global reduction in autophagy is associated with reduced plasma membrane degradation and ageing of the epidermis (Scherfer *et al*, 2013).

Here, we directly tested the connection between autophagy and syncytium formation during wound healing and in the unwounded epidermis. We show that in *Drosophila* larvae elevated autophagy induces syncytium formation by membrane breakdown both in the epidermis and during epidermal wound healing.

Results

Autophagy and syncytium formation during wound healing

To analyse the function of autophagy for wound healing, we co-expressed a marker for autophagosomes (*GFP-Atg8a*) with RNA interference (RNAi) constructs against autophagy components in the epidermis and created epidermal wounds in early third larval instars. *Atg8a* is homologous to human MAP1 LC3 and localizes to all autophagic vesicles from the phagophore to the autolysosome (Klionsky *et al*, 2021). In unwounded control epidermis, *GFP-Atg8a* is diffusely distributed in the cytoplasm and nucleus and is additionally seen in a few puncta in the cytosol (Fig 1A). After wounding, new autophagosomes appear in the cells surrounding the wound (Kakanj *et al*, 2016), increasing in number until completion of wound closure and starting to drop again to 50–60 min after wound closure (Fig 1A–C, Appendix Fig S1 and Movies EV1 and EV2).

When autophagy was suppressed by knockdown of *Atg1* (the key component for autophagy initiation) or *Atg5* (a component for phagophore elongation) in the epidermis, the number of *Atg8a* vesicles in the cells around the wound was significantly reduced (Fig 1A, B and D, Movie EV1). Knockdown of *Atg6* (phagophore nucleation factor), *Atg7* or *Atg12* (phagophore elongation factors) also resulted in a decrease in autophagosomes, but the effect was

much less pronounced (Fig 1A, B and D, Movie EV1). Our data for *Atg7* and *Atg12* knockdown are consistent with previous findings that these components are accessory but not necessarily essential for the completion of autophagy (Schwenzfeier, 1991; Scott *et al*, 2004; Chang *et al*, 2013; Scherfer *et al*, 2013; Xu *et al*, 2015). However, the mild effect of *Atg6* knockdown might be the result of a less effective RNAi construct, since *Atg6* has been shown to be essential for autophagy. (Shravage *et al*, 2013; Xu *et al*, 2015).

We analysed the effect of suppressing autophagy (using RNAi against *Atg1*, *Atg5*, *Atg6*, *Atg7* or *Atg12*) on the quality and rate of wound healing in larvae in which the plasma membranes were marked with Src-GFP or the adherens junctions with *DE-Cadherin-GFP* and the myosin regulatory light chain (MRLC) with *Sqm-Cherry* (a tagged form of *Drosophila* MRLC). Epidermal reduction of autophagy caused no morphological or developmental abnormalities in the epidermis and it did not affect the quality or rate of wound healing: lamellipodia, cell crawling, the assembly and contraction of the actomyosin cable, and the rate of wound closure were all normal and similar to controls (Fig 1E and F, Movies EV3 and EV4).

In the larva, the cells surrounding a wound form a large syncytium (Galko & Krasnow, 2004; Wang *et al*, 2015). To visualize syncytium formation in our experimental system, we created wounds in larvae with epidermal mosaics of cells expressing free cytosolic GFP (Fig 2A and B). When we ablated an unmarked cell that was surrounded by both GFP-marked and unmarked cells, GFP gradually appeared in initially GFP-free cells around the time of wound closure (Fig 2B and Movie EV5). By the time the wound was fully closed, all cells surrounding the wound were GFP positive, with an overall homogeneous GFP level. This behaviour was independent of the initial number of GFP-positive cells.

We confirmed that the appearance of GFP in the initially GFP-negative cells was not due to *de novo* synthesis in response to wounding. When we ablated a cell that was surrounded by cells without GFP we observed no GFP expression during an imaging time of ~3 h (Fig 2C and Movie EV6A). When we only damaged the apical membrane of a cell without fatally wounding it, the GFP-negative cells surrounding the damaged cell remained GFP negative (Fig 2D and Movie EV6B). This indicates that our experimental manipulations do not induce *de novo* GFP expression in GFP-negative cells around the wound. Instead, we conclude that the GFP is redistributed from GFP-expressing to GFP-negative cells, and that the wound-healing response includes a process by which the cells around the wound gradually share their cytoplasm.

One possible explanation for the observations so far is that the redistribution of cytoplasm and the induction of autophagy observed during wound healing are causally related. We tested this by ablating cells in epithelia in which *Atg1* or *Atg5* were knocked down and GFP was expressed in single or multiple clonal cells. We saw no intercellular redistribution of GFP in these experiments (Fig 2B and Movies EV7 and EV8). Thus, a clonal cell that is *Atg1* or *Atg5* deficient in a wild-type background does not share its content with the neighbouring cells. This shows that cytoplasmic mixing and the formation of a syncytium depend on autophagy and that autophagy is required in a cell-autonomous manner for a cell to become part of the syncytium.

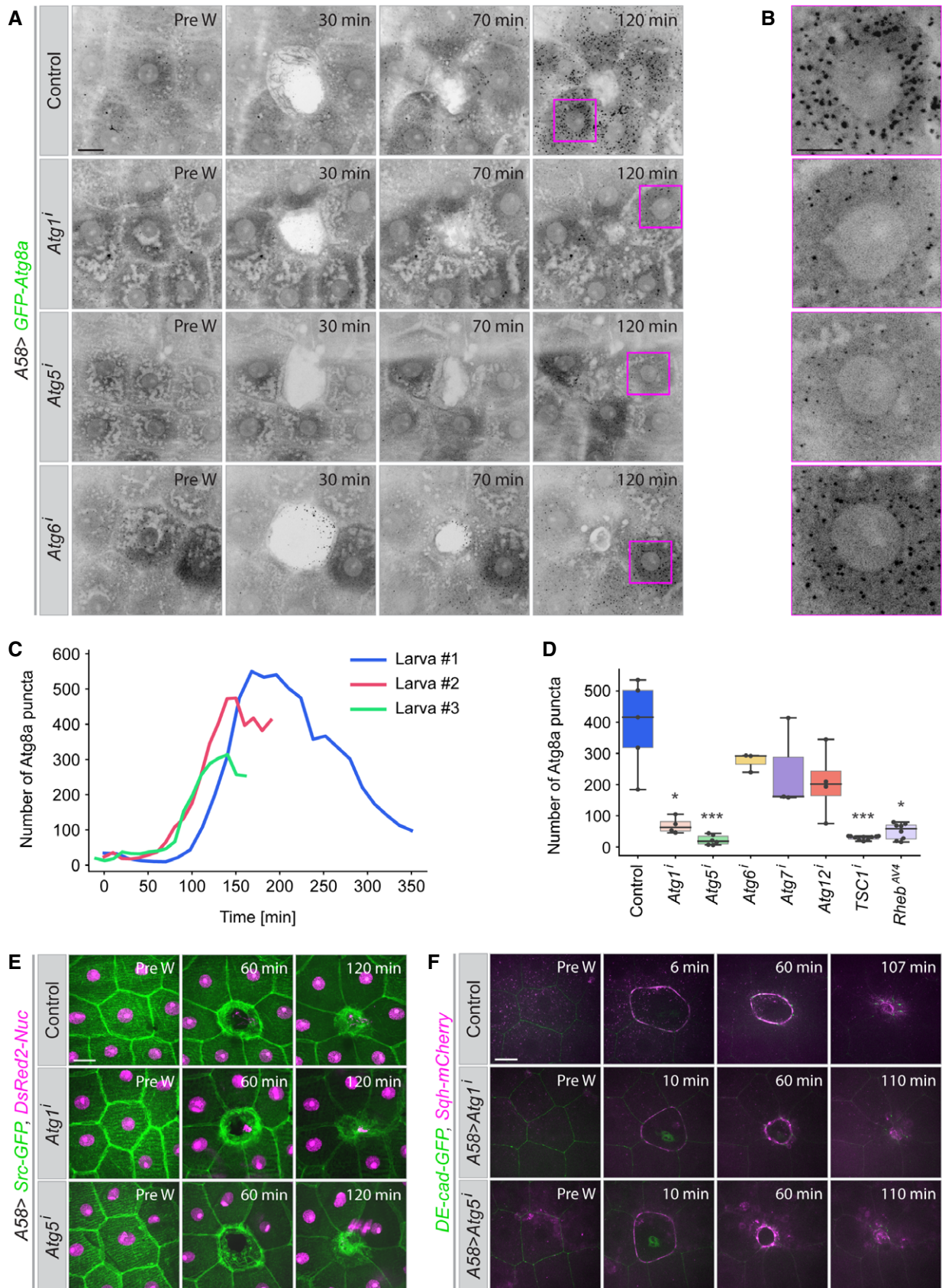


Figure 1.

Figure 1. Autophagy during epidermal wound healing.

A–D Appearance of autophagic structures (marked with GFP-Atg8a) during wound closure in the epidermis of control third instar larvae and after epidermal knockdown of the autophagy pathway components Atg1, Atg5, Atg6, Atg7 or Atg12. All constructs are expressed in the epidermis under the control of the *A58-Gal4* driver. (A) Time points from movies of wounded epidermis. The wounds have closed by 2 h in all cases. (B) Higher magnification of the areas marked by magenta boxes at $t = 120$ min. (C) Quantification of the appearance of GFP-Atg8a puncta in the imaged area ($10,000 \mu\text{m}^2$) 3 control larvae, shown for each individual larva. (D) Quantification of number of GFP-Atg8a puncta in different genetic conditions measured in an area of $10,000 \mu\text{m}^2$ at the time of wound closure; $n = 4$ –10 larvae each genotype, for the detail see Data analysis. We assumed unequal sample size and unequal variances and calculations were performed. Values are presented as box plots. Box plot elements are: centre line, median; box limits, upper and lower quartiles; whiskers, $1.5 \times$ interquartile range; points, outliers. For statistical hypothesis testing, independent and non-parametric (Kruskal–Wallis) t -tests were performed for the mean number of spots in control and experimental conditions. P -values are indicated as follows: $*P < 0.04$; $***P < 0.0002$ and lack of an asterisk means non-significant ($P > 0.123$).

E, F Effect of suppressing autophagy on wound healing and actin cable formation. Time-lapse series of single-cell wound healing in larvae expressing (E) Src-GFP (green) and DsRed2-Nuc (magenta) to mark cell membrane and nuclei and (F) endogenously GFP-tagged E-cadherin (DE-cad-GFP; green) and mCherry-marked myosin regulatory light chain (Sqh-mCherry; magenta) to visualize adherens junctions and actomyosin cables.

Data information: (A, B, E, F) Z-projections of time-lapse series in early L3 larvae, $n = 9$ –15 larvae each genotype. Scale bars, A, E, F, $20 \mu\text{m}$ and B, $10 \mu\text{m}$. Pre W: pre-wounding. Images from Movies EV1–EV4. Genotypes of all images are listed in Table 2.

Source data are available online for this figure.

Effect of Autophagy on epidermal morphology

We also analysed the effect of autophagy induction in the unwounded epidermis. The basal level of autophagy is low and only few Atg8a-positive vesicles are detected in the epidermis of control larvae (Fig 3A and B). We activated autophagy artificially with two different overexpression constructs for Atg1, Atg1^{GS} and Atg1^{6B} (Table 1 and Scott *et al*, 2007). Atg1^{GS} and Atg1^{6B} were originally called “weak” and “strong,” respectively (Bjedov *et al*, 2020), but we found that in the larval epidermis their effects are practically indistinguishable. Both Atg1^{GS} and Atg1^{6B} led to an increase in the number of Atg8a vesicles (Fig 3A–E). We also observed an increase in vesicles marked with LAMP1-GFP, an endo-lysosomal marker, indicating that the entire autophagic pathway was active (Appendix Fig S2A and B).

Autophagy is normally kept inactive via TORC1 signalling, and we tested the effect of both disruption and activation of TORC1 on autophagy. Experimental activation of TORC1, either through overexpression of an upstream activator, *Rheb^{AV4}* or knockdown of the TORC1 inhibitor, *TSC1* (*TSC1^l*), had little effect on the number of Atg8a-positive vesicles in the tissue (Fig 3A–C). In contrast, expression of the TORC1 antagonists, *AMPK α ^{CA}*, *TSC1*, *TSC2* or a dominant-negative version of Tor (*Tor^{DN}*), or downregulation of *Tor* or *raptor* by RNAi increased the number of Atg8a-positive and LAMP1-positive vesicles (Fig 3A–C and Appendix Fig S2A and B). Epidermal knockdown of *rictor*, a component of TORC2, did not induce autophagy (Fig 3A–C and Appendix Fig S2A and B). Thus, the suppression of autophagy in the larval epidermis depends specifically on TORC1.

Transmission electron microscopy (TEM) images showed large numbers of autophagosomes and autolysosomes after TORC1 reduction or Atg1 overexpression while very few were present in control epidermis confirming that the increase in Atg8a- and LAMP1 puncta corresponded to an increase in autophagosomes and autolysosomes (Fig 3D and E).

The increase in Atg8a-positive vesicles caused by overexpression of Atg1 was always similar in quality but stronger in extent than that resulting from reducing TORC1 activity directly or through its upstream regulators.

In the experiments above we noticed that cells often appeared morphologically abnormal. We then used the plasma membrane marker Src-GFP to analyse this effect. Reduction in TORC1 activity or expression of Atg1 led to distortions of epidermal morphology,

with effects on the shape and orientation of cells, localization of the nuclei, and size heterogeneity in cells and nuclei (Fig 3F). Most strikingly, cell outlines often appeared to be interrupted or missing altogether (Fig 3F). Time-controlled transgene activation using the temperature-sensitive Gal80^{ts} system showed that defects were visible within 6 h of TORC1 depletion or activation of Atg1 (the earliest possible time point for analysis, since the marker constructs were not detectable sooner). These defects became exacerbated over the following 18 h, with a progressive change in organization of lateral membranes, accompanied by the formation of large vesicles that moved towards the centre of the cell and then disappeared (Fig 3G and H, Appendix Fig S2C and Movie EV9). Together, these results indicate that disruption of TORC1 signalling causes exacerbated autophagy and altered epidermal morphology.

Autophagy and the formation of epithelial syncytia

The results so far could mean that the missing cell outlines were due to a change in membrane properties, so that Src-GFP could no longer be recruited, or there could be gaps or defects within the membranes. To distinguish between these possibilities, we first examined other membrane markers. The main components of the apical cell polarity complex Par3 (Bazooka) and aPKC, normally located in the apical domain of the lateral plasma membrane, and the septate junction proteins, Fasciclin III (FasIII) and Neuroglian (Nrg), all showed abnormal distributions or were absent over large areas in TORC1-depleted and Atg1-expressing epithelia (Fig 4A–C and Appendix Fig S3A–D). Both live imaging with GFP constructs and immunofluorescence of fixed material gave the same results, showing that mislocalization of GFP or the absence of determinants was neither due to breakdown of GFP nor due to fixation problems.

To assess the extent of cell abnormality, we also imaged other molecules involved in cell shape and polarity. We found that adherens junctions (visualized with DE-Cadherin-GFP) were reduced or absent, while myosin (MyoII, visualized with the mCherry-tagged non-muscle type II myosin regulatory light chain, Sqh-mCherry) had formed strong cortical and cytosolic filaments (Fig 4D). Experimental activation of TORC1 had the opposite effect: it reduced myosin level similar to knockdown of RhoA or Rok (Appendix Fig S3E).

TORC2 is involved in the regulation of plasma membrane and actin cytoskeleton homeostasis both in yeast and mammalian cells

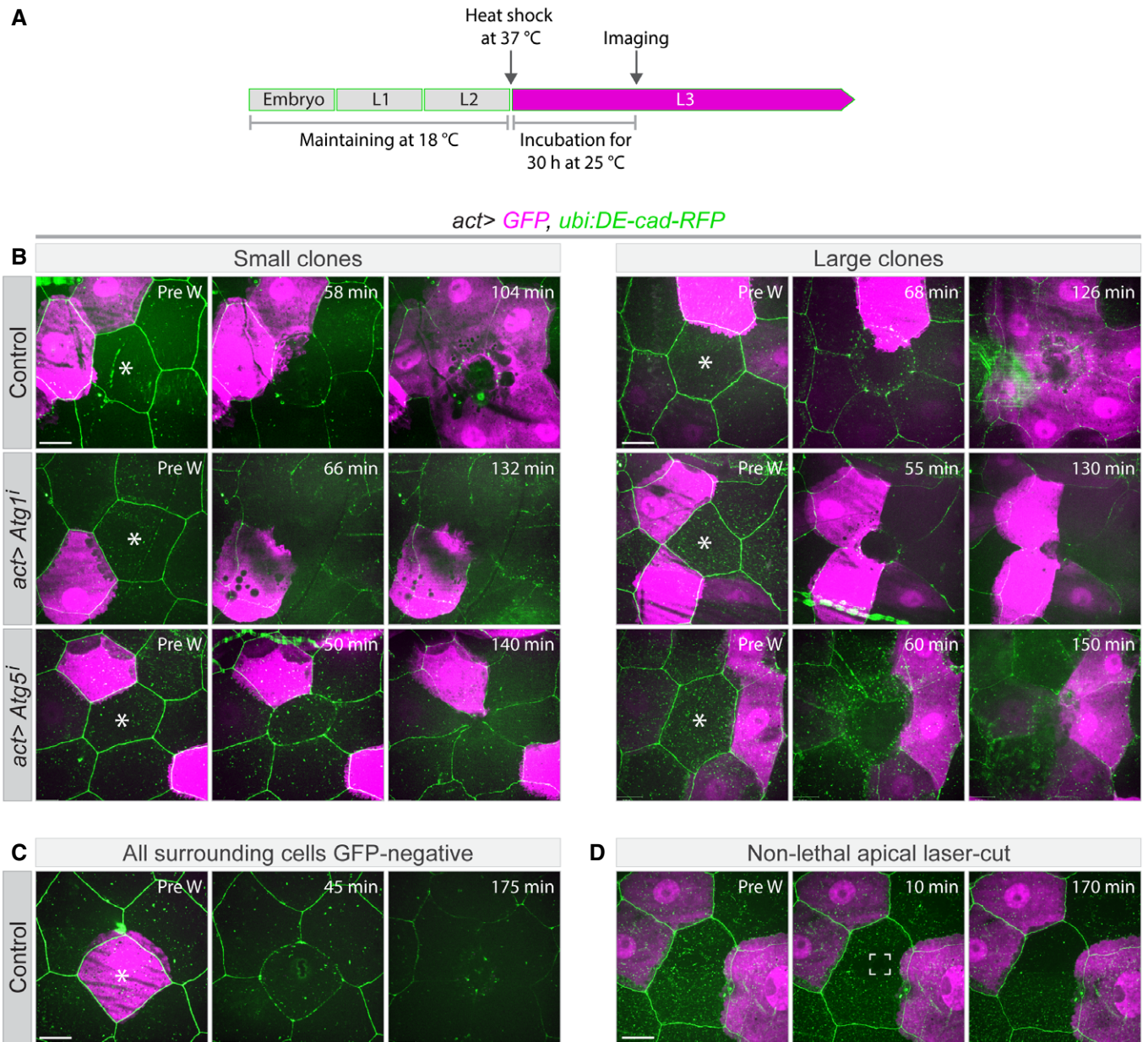


Figure 2. Syncytium formation during wound healing.

A Schematic for timing of transgene expression and start of live imaging. Gene expression was induced at the end of the second larval instar, laser ablation and imaging started 30 h later.

B Wound healing in epithelia with clonally expressed cytoplasmic GFP (magenta) under the *actin5c-Gal4* driver in control larvae (*act>GFP*) or larvae expressing RNAi constructs specific for *Atg1* or *Atg5*. Laser-ablated cells are marked with white asterisks. To visualize cell borders DE-cad-RFP (green) was expressed in all tested genotypes. By the end of wound closure, GFP from the clonal cells has spread to all cells around the wound in the control, but not if autophagy is suppressed, regardless of the number of cells initially expressing GFP.

C Control larva in which a GFP-expressing cell was wounded. No GFP is induced in or taken up by the surrounding cells.

D Control experiment in which the central cell was damaged but not killed (white marked area). No wound response occurs and no GFP leakage between neighbouring cells is seen.

Data information: (A–D) $n = 6–9$ larvae each genotype. The control pre-wounding small clone in b (top left panel) is from Kakanj et al, 2016. B, C, D, z-projections of time-lapse series. B–D, Scale bars, 20 μ m. Pre W: pre-wounding. Images from Movies EV5–EV8.

(Riggi et al, 2018, 2020), but reduction of TORC2 activity had no effect in any of the assays we used for autophagy or cell morphology (Figs 3A–C and F, and 4A and D, Appendix Fig S2A and B).

Z-sections of cells expressing Src-GFP or the transmembrane marker mCD8-GFP showed that the basal and apical membranes appeared intact (Appendix Fig S4A and B). We stained also for the

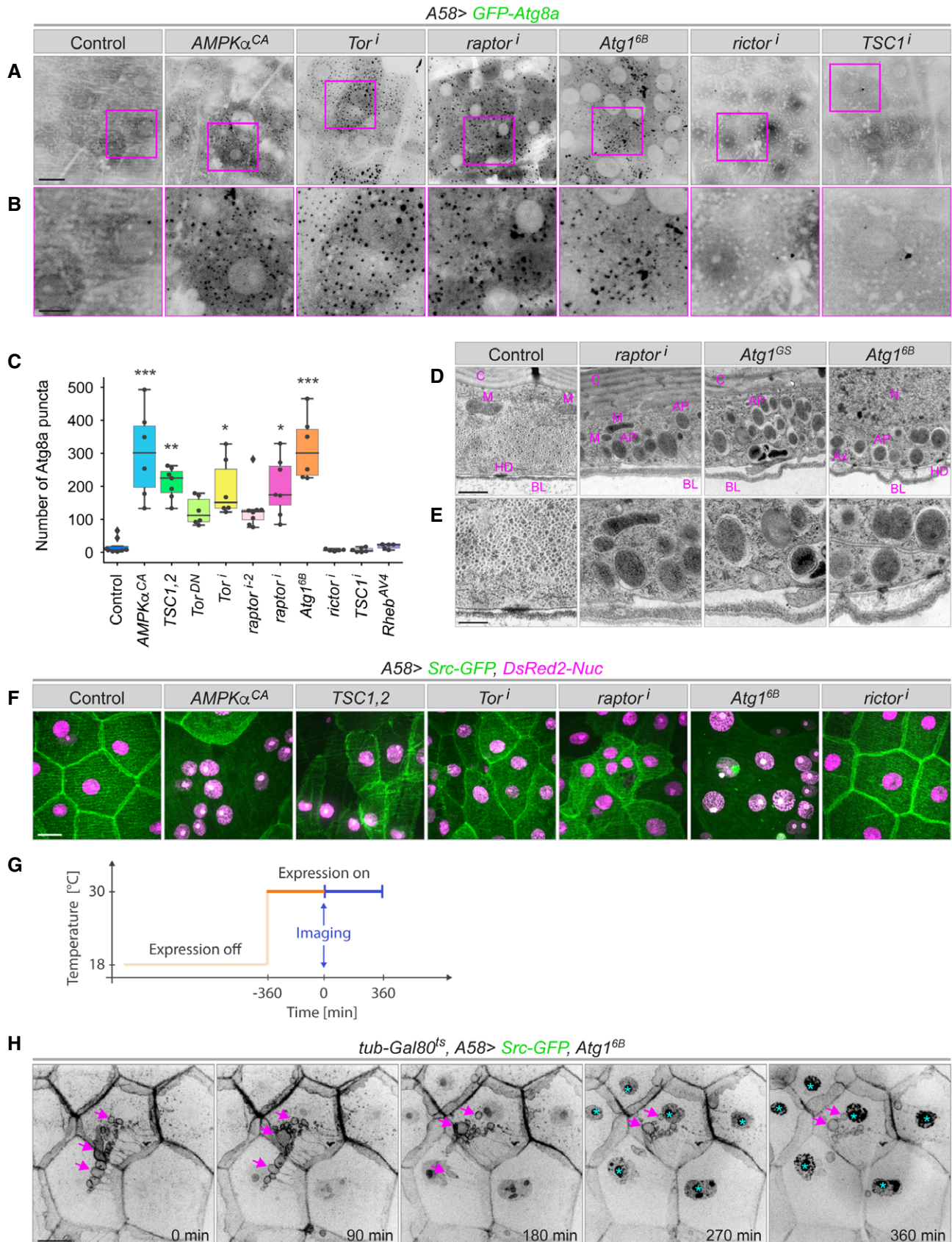


Figure 3.

Figure 3. Autophagy in unwounded epidermis.

- A–E Control of epidermal autophagy by TOR signalling. (A) Epidermis of third instar larvae expressing the autophagosome marker GFP-Atg8a together with constructs for up- or downregulating the autophagy pathway in the epidermis. Healthy epidermis contains few autophagosomes, but artificially activating autophagy through overexpression of Atg1 or blocking TOR signalling leads to accumulation of autophagosomes. (B) Higher magnification of the areas marked by magenta boxes in (A). (C) Quantification of Atg8a puncta in an area of 10,000 μm^2 , $n = 6–8$ larvae each genotype. We assumed unequal sample size and unequal variances and calculations were performed. Values are presented as box plots. Box plot elements are: centre line, median; box limits, upper and lower quartiles; whiskers, 1.5 \times interquartile range; points, outliers. For statistical hypothesis testing, independent and non-parametric (Kruskal–Wallis) t -tests were performed for the mean number of spots in control and experimental conditions. P -values are indicated as follows: * $P < 0.04$; ** $P < 0.003$; *** $P < 0.0002$ and lack of an asterisk means non-significant ($P > 0.123$). (D, E) Transmission electron micrographs of sections through the epidermis of larvae with elevated autophagy at two different magnifications. AP: autophagosome; Ax: cross-section of an axon; BL: basal lamina; C: cuticle; HD: hemidesmosome; M: mitochondrion; N: nucleus.
- F Disruption of epidermal morphology after upregulation of autophagy. The membrane marker Src-GFP is lost from large areas of the epidermis and nuclei have lost their regular spacing. Image in control and *ric1* panels are from the time laps in Appendix Fig S5B and Movie EV12.
- G Schematic for temporally controlled transgene expression and imaging in (H). Gene expression is induced at the end of the second larval instar, live imaging started 6 h later and continued for an additional 6 h.
- H Example of membrane dynamics after time-controlled Atg1^{6B} expression. Src-GFP containing material appears to be taken out of and eventually detached from lateral cell membranes (arrows). Over the period of observation, abnormal accumulation of GFP is seen in the nuclei (cyan asterisks). $t = 0$ is 6 h after *A58-Gal4* activation. Image from Movie EV9.

Data information: A, B, F, H, z-projections; $n = 20–50$ larvae each genotype. Scale bars: A, F, H, 20 μm , B, 10 μm , D, 1 μm and E, 500 nm. Source data are available online for this figure.

basal marker β -integrin, which is normally localized at the basal and basolateral plasma membrane up to the border of the septate junctions (Fig 4E and Appendix Fig S4C). Because the lateral membrane is highly folded (Fig 4F), the outlines of cells are seen as a fuzzy band of increased integrin staining. The epithelium is very thin and the nuclei extremely flattened, but in spite of the low-resolution, z-sections show the integrin signal in a thin line below the nuclei in control epidermis. This separation is less clear in the absence of TORC1 signalling, and strongly disturbed when Atg1 is overexpressed. In this case, integrin is seen both below and above the nuclei, suggesting that it is also present in the apical compartment (Fig 4E).

The basal membrane is not only present, but is also intact as shown by the fact that we see no significant loss of cytosolic GFP from the epidermis, either in untreated or in wounded epithelia (see below). This may also explain why these larvae can survive throughout larval development.

Finally, despite defects in the lateral plasma membranes, the abnormal epithelia resulting from uncontrolled autophagy were able to form an actomyosin cable around wounds. While the wounds healed more slowly, they eventually closed completely, and most of the larvae (~75%) survived to the pupal stage (Appendix Fig S5A and B and Movies EV10–EV12). Thus, the defects in morphology are not simply a sign of the epithelium disintegrating or dying, but the epithelium is viable and physiologically active.

The results so far indicate that activation of autophagy results in the disappearance of lateral membrane markers. If this is due to the loss of lateral membrane then cytosolic proteins should be able to diffuse between cells. We tested this with fluorescence loss in photobleaching (FLIP) to monitor the intercellular movement of GFP. In control experiments, we bleached the GFP in an area of 179 μm^2 within a cell for 3 min, resulting in the removal of GFP not only from the bleached area but also from the entire cell (Fig 5A–C and Movie EV13A). The GFP in neighbouring cells was not affected, and no GFP re-appeared in the bleached cell over the next 20 min. In contrast, a 3-min illumination of an area of 179 μm^2 in larvae expressing Atg1 in the epidermis was insufficient to remove GFP from the marked area (Fig 5A–C and Movie EV13B). Photobleaching of a larger area (1,098 μm^2 ; 1–4 nuclei) led to the removal of GFP

from this area, but the area remained dark only for a few seconds, after which the fluorescence signal re-equilibrated to the same level as the surrounding area, which we interpret as diffusion of GFP into the bleached region from neighbouring areas (Fig 5A–C and Movie EV13C). Z-sections of movies showed clear diffusion of GFP laterally within the epithelium, and never any basal or apical leakage (Movie EV14). This also indicates that the barrier function of the epidermis is not compromised.

To assess the extent of the region connected to the bleached area, we increased the time of photobleaching to 20 min (Fig 5A, B and D, Movie EV15). This led to an ~85% reduction of the GFP signal in a much larger area (7,000–15,000 μm^2 , with 10–24 Nuclei), showing that the epidermal cells in this patch had formed an extended syncytium from which GFP entered the area being bleached. In most cases the fluorescence signal did not recover over the next 20 min, showing the syncytium had been exhausted of GFP and was separated from other parts of the epidermis. Thus, activation of autophagy induces the formation of syncytial patches in the unwounded epidermis.

Furthermore, transmission electron micrographs showed that lateral membranes were missing in many places (as judged by adjacent nuclei not being separated by a membrane), but the basal membrane was intact (Fig 5E and F). The epithelium also showed a range of other defects, from an abnormal basal lamina and apical cuticle to deformed nuclei (Appendix Figs S6A and B and S8B and C).

The effect of uncontrolled autophagy on cell morphology was not unique to the epidermis. The ectodermal driver (*A58-Gal4*) also directs expression in the tracheal system, and the tracheal trunk and branches were severely distorted (Appendix Fig S6C). Similarly, in experiments where autophagy was induced in enterocytes of the gut and secretory cells of salivary glands (using *NP1-Gal4*), these epithelia also lost lateral membrane markers and had abnormal shapes (Fig 6A and Appendix Fig S6D and E). Yet, as in the epidermis, the epithelial barrier function was not compromised, as confirmed by a Smurf barrier assay (Fig 6B).

Together, these experiments indicate that activation of autophagy affects the lateral membrane of the epidermal cells leading to the formation of syncytia in the unwounded epidermis, which appears reminiscent of the syncytium observed during wound healing. Both loss of TORC1 and hyperactivity of Atg1 disrupt cell integrity in a

specific manner: lateral membranes are lost, but basal and apical membranes remain intact but adopt inappropriate identities. As a consequence, autophagy must be kept repressed in epithelia for cell integrity and polarity to be retained, and this repression requires TORC1 activity.

TORC1-dependent autophagy alleviates nuclear defects in models of laminopathy

To investigate whether other membranes were affected by uncontrolled autophagy, we used fluorescent markers for the mitochondria (mito-GFP), ER (KDEL-RFP), Golgi (GalT-GFP) and nuclear envelope (endogenously GFP-tagged Kugelkern (Kuk), a *Drosophila* nuclear lamina protein). Reduction of TORC1 or expression of Atg1 had no apparent effect on the number or distribution of the mitochondria (Appendix Fig S7A). This fits with TEM images, which show a normal density and morphology of mitochondria. However, the number of KDEL- and GalT-positive puncta was reduced, suggesting that they were also being depleted by autophagy (Appendix Fig S7B–E).

Nuclei marked with GFP-Kuk in control cells appear round with a homogeneous GFP signal at the lamina (Fig 7A). Loss of TORC1 or Atg1 hyperactivation caused abnormalities in nuclear morphology and shape, disruption of the nuclear membrane with irregular GFP distribution and vesicular structures inside and outside of the nucleus (Fig 7A and Appendix Fig S8A). Other markers associated with the nuclear lamina were also abnormal. Bazooka/Par3, normally localized at the nuclear envelope, was not detectable when autophagy was activated in epidermal cells (Fig 4A and Appendix Fig S3A). TEM imaging supported these observations, in addition showing autophagosomes within the nucleus (Appendix Fig S8B and C). The defects were not restricted to nuclear morphology but extended to chromatin organization: an RFP-tagged version of His2Av (*endo:His2Av-mRFP1*) revealed abnormal chromatin condensation in cells with upregulated autophagy (Appendix Fig S8D and Movie EV16).

Defects in the nuclear lamina are associated with a spectrum of diseases known as laminopathies (Worman & Courvalin, 2005; Brandt *et al*, 2006; Scaffidi & Misteli, 2006; Polychronidou & Grobans, 2011). In a *Drosophila* model for nuclear laminopathy, overexpression of Kuk or Lamin B (LamB) leads to the lobulation and increased folding of the nuclear envelope in the muscle and a reduced lifespan (Brandt *et al*, 2008; Polychronidou *et al*, 2010; Polychronidou & Grobans, 2011; Petrovsky *et al*, 2018). Overexpression of GFP-Kuk or RFP-LamB in the epidermis also caused an abnormal morphology of nuclei but the larvae developed to fertile

adult flies, without visible defects (Fig 7B and Appendix Fig S8E). Induction of autophagy by TORC1 reduction or Atg1 overexpression largely reduced the nuclear defects caused by elevated levels of Kuk or LamB (Fig 7B and Appendix Fig S8E), pointing to the possibility of the autophagy machinery competing for the membrane needed to increase the nuclear envelope. Conversely, this shows that elevated autophagy likely also depletes the nuclear envelope, possible via the ER. Thus, autophagy can counteract the nuclear defects seen in this laminopathy model.

Relevance of autophagy for plasma membrane integrity

We have seen that reduction of TORC1 induces autophagy and causes similar defects in epidermal cells as the more direct activation of autophagy by Atg1 does. Next, we tested whether TORC1 acts exclusively through inducing autophagy, and if so, whether the entire autophagic process has to be completed for the membrane defects to occur. Apart from repressing Atg1 activity, TORC1 also activates S6K. Constitutive activation of S6K (*S6K^{CA}*) did not improve any aspect of cellular defects caused by the TORC1 block, indicating that loss of S6K activity is not responsible for the defects caused by loss of TORC1 (Appendix Fig S9A). TORC2 reduction also did not improve any of the cellular defects derived by TORC1 reduction (Appendix Fig S9A).

To assay the different steps of the autophagic pathway, we first tested the efficiency of RNAi constructs in suppressing autophagy in the epidermis. As during wound healing, knockdown of *Atg1* or *Atg5* both reduced the number of Atg8a-positive vesicles in TORC1-depleted epidermis to control levels (Appendix Fig S9B and C). In contrast, knockdown of *Atg6* or *Atg7* reduced the number of Atg8a-positive vesicles only slightly, similar to their limited effect on autophagosomes during wound healing (Appendix Fig S9B and C and Fig 1D). These two were, therefore, not suitable as tools to block later stages of autophagy in this system.

To test whether the effects of TORC1 on cell membrane were caused exclusively through the release of Atg1 activity and the autophagy pathway, we downregulated *Atg1* or *Atg5* together with TOR or raptor. In these larvae, the membrane defects caused by uncontrolled autophagy were largely abolished, except in a few cells at segment borders (Fig 8A and Appendix Fig S10A). The suppression of the effects of TORC1 knockdown is not due to titration of Gal4 activity because other constructs such as *UAS-rictor²* or *UAS-S6K^{CA}* did not have this effect (Appendix Fig S9A). This shows that Atg1 is needed to mediate the effects of TORC1 on lateral membranes. Similarly, downregulation of *Atg5* suppressed the effects of both TORC1 reduction and Atg1 hyperactivity (Fig 8A and

Figure 4. Effect of uncontrolled autophagy on plasma membrane-associated proteins.

- A–E Surface views (A–D) and z-sections (E) of third instar larval epidermis expressing the indicated fluorescent markers and RNAi or overexpression constructs. (A) Bazooka/Par3, normally seen at the apical adherens junction and in a perinuclear position, is lost or reduced in large areas under uncontrolled autophagy as are lateral membrane markers, (B) Fasciclin-III (FasIII), (C) neuroglian (Nrg) and (D) adherens junctions (DE-cad), whereas large bundles decorated with MRLC appear. (E) The baso-lateral transmembrane protein β -integrin is not lost; in extreme conditions, it is seen in both the apical and basal membranes (overexpression of Atg1^{6B}). Arrows in the z-sections point to high accumulation of integrin along the folded lateral membranes.
- F Electron micrograph of a section through the larval epidermis to show the highly folded lateral junction between two epidermal cells (magenta and cyan). Left, cartoon; middle, false colouring; right, original image. C: cuticle; M: mitochondrion; BL: basal lamina; AJ: adherens junction; SJ: septate junction; GJ: gap junction, N: nucleus, Mv: apical microvilli connecting the cuticle to the cell.

Data information: A–E, $n = 15$ –40 larvae each genotype. Scale bars: A–E, 20 μm and F, 2 μm . Images from Movies EV10 and EV11.

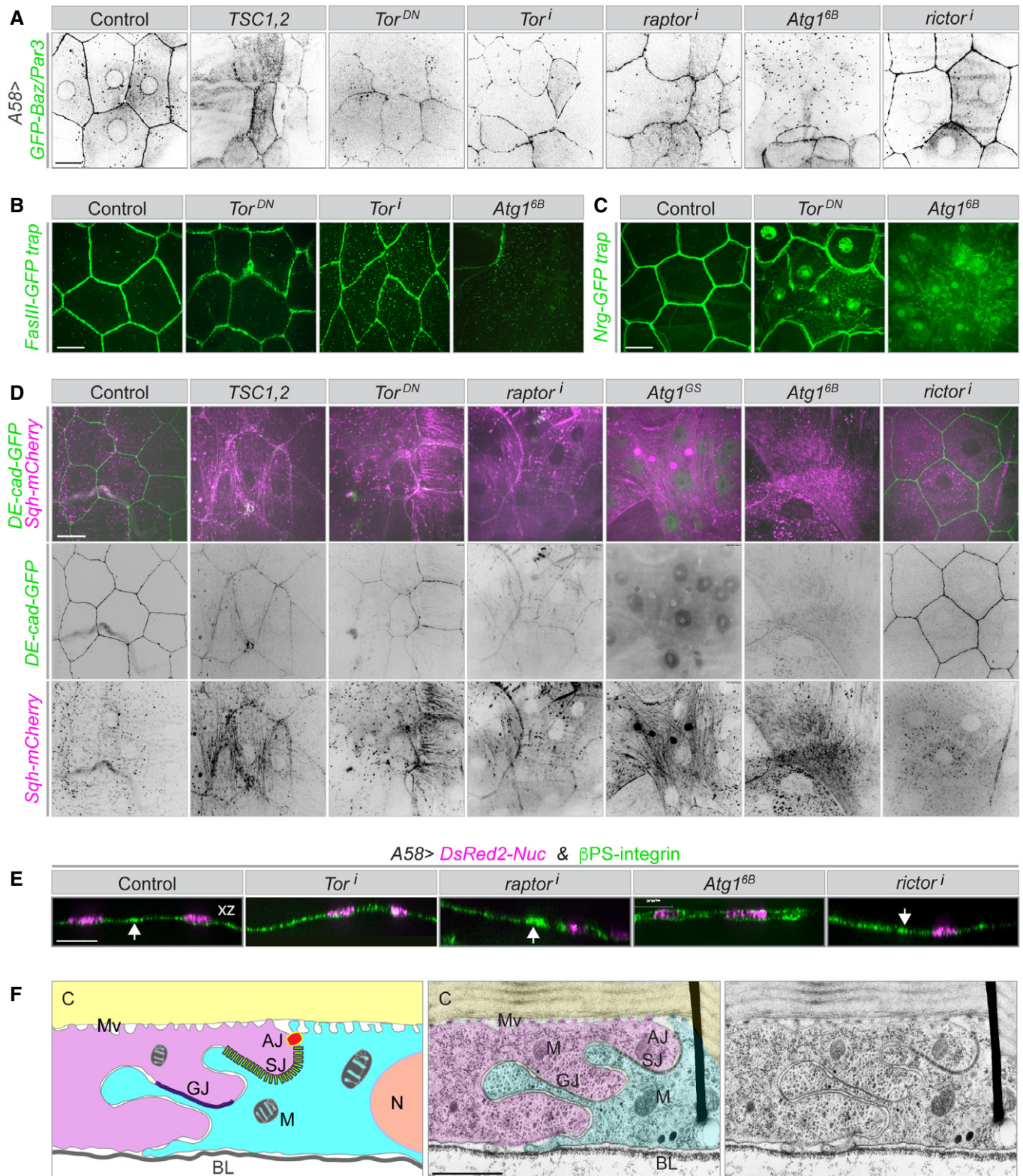


Figure 4.

Appendix Fig S10A). We also confirmed with the FLIP assay that syncytium formation was reduced in *Atg1^{GS}*, *Atg5ⁱ* larvae. GFP was no longer able to move into bleached areas from large surrounding

regions; instead, only one cell was bleached, as in controls, or at most one neighbouring cell also lost fluorescence (Fig 8B–D and Movie EV17). Blocking autophagy also re-established the proper

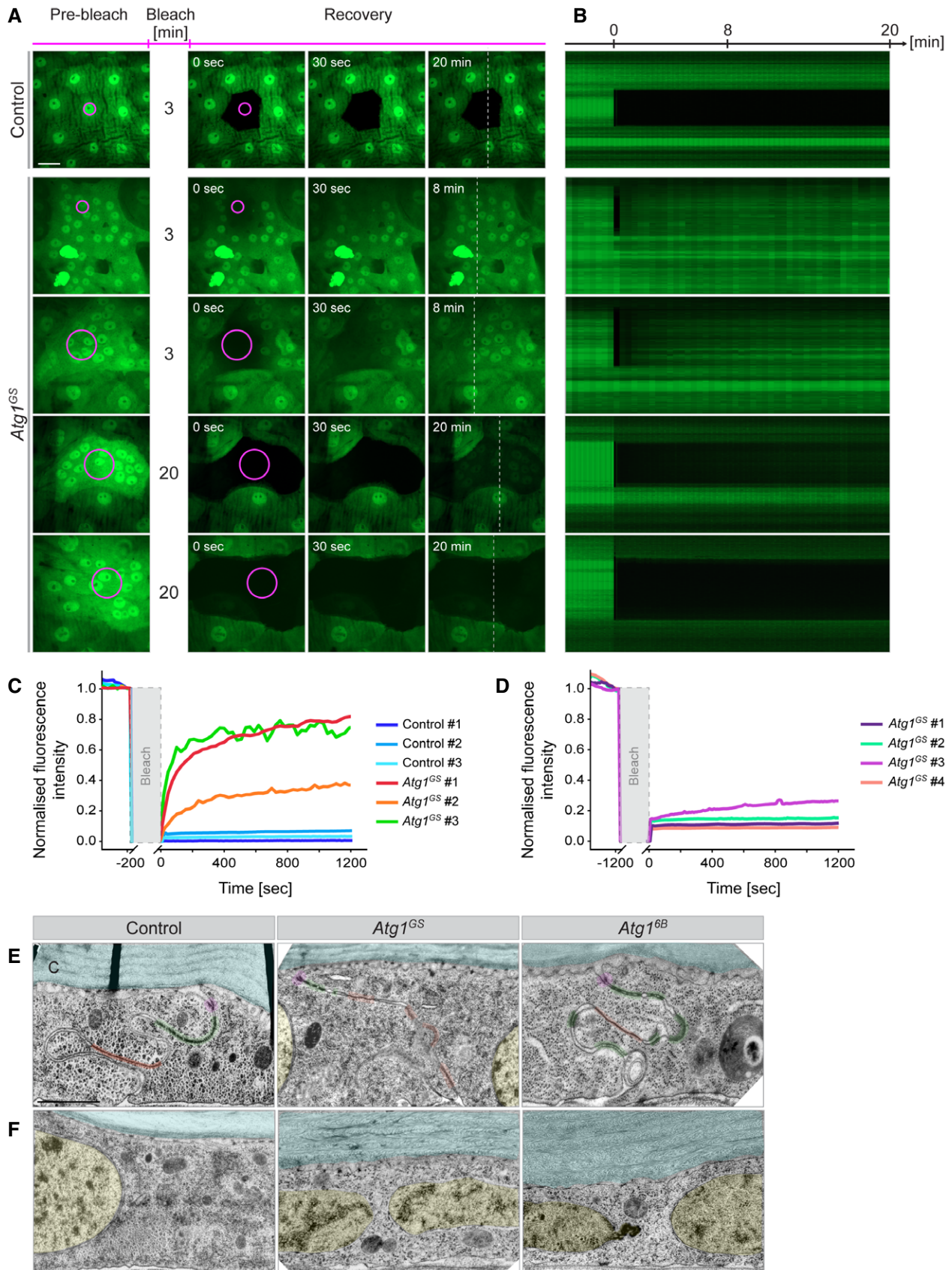


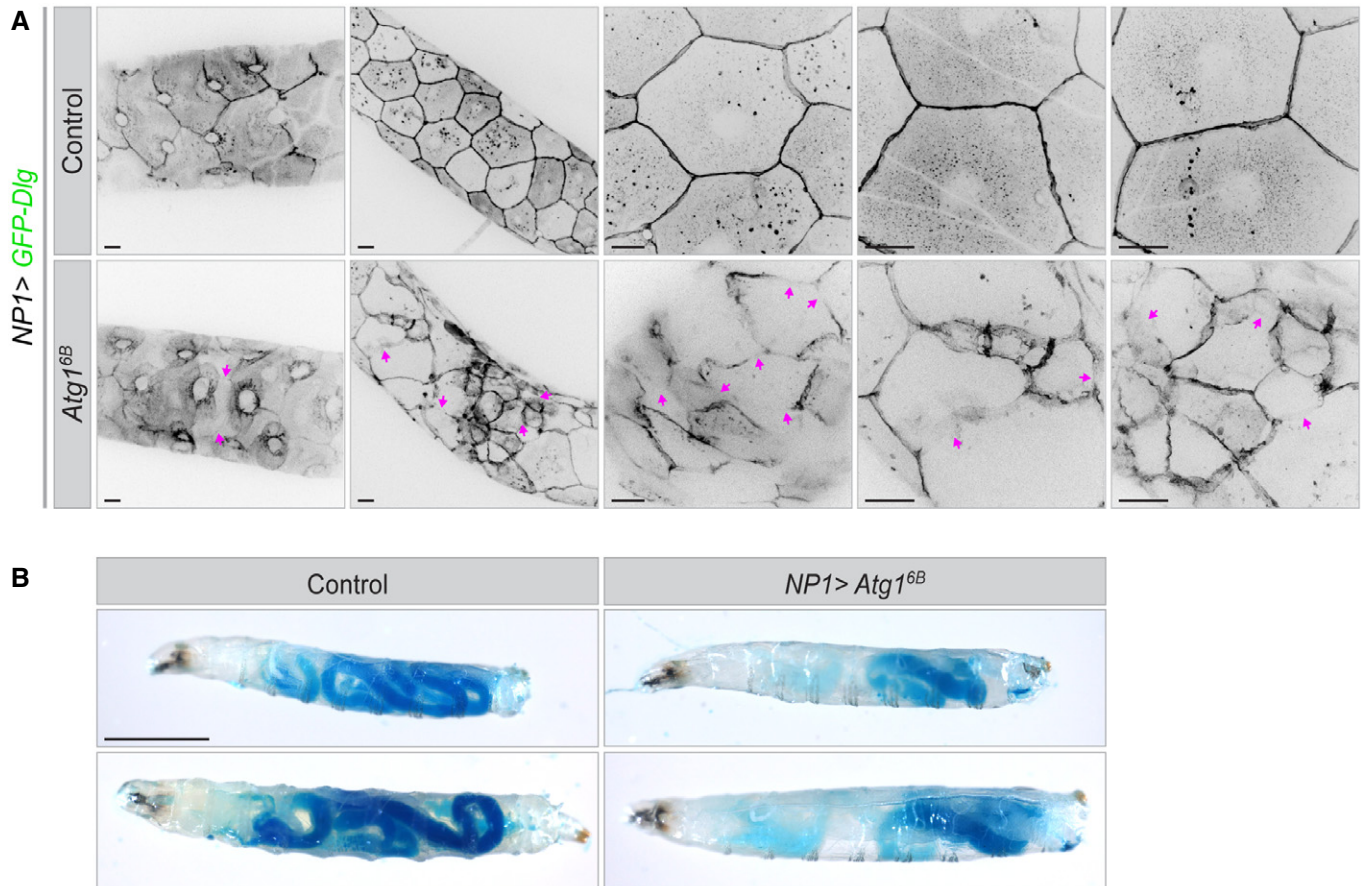
Figure 5.

Figure 5. Loss of lateral membrane integrity.

A–D Fluorescence loss in photobleaching (FLIP) to test free cytoplasmic GFP motility within the epidermis. A small area (magenta circle; 179 or 1,098 μm^2) was laser-illuminated for the indicated times (3 or 20 min) in control or Atg1-expressing epidermis also expressing free GFP. (A) Snapshots before bleaching and at 3 points of recovery. (B) Kymographs along the broken line in (A) during recovery. (C, D) Quantification of fluorescence recovery after bleaching, shown separately for 3 and 20 min bleaching protocols.

E, F Electron micrographs showing morphological defects or absence of lateral cell membranes in epithelia with upregulated autophagy. (E) Membrane domains with tight apposition between neighbouring cells are marked in magenta (adherens junctions), green (septate junction) and orange (gap junctions). (F) Nuclei (yellow) and lateral membranes in healthy epidermal cells cannot be shown in one image because they are too far apart, whereas when autophagy is upregulated, nuclei are often found close together and not separated by plasma membranes. C: cuticle (blue).

Data information: A–D $n = 5–9$ larvae for each FLIP protocol. Scale bars: A, 20 μm and E, F, 2 μm . Images from Movies EV13–EV15. Source data are available online for this figure.

**Figure 6. Effect of uncontrolled autophagy on gut enterocytes and barrier function.**

A Larval gut epithelia in which enterocytes express a marker for polarity and septate junctions, GFP-Dlg using the *NP1-Gal4* driver together with or without *Atg1^{6B}*. Expression of *Atg1^{6B}* leads to disruption of lateral plasma membrane (magenta arrows). $n = 32–44$ larvae each genotype.

B Smurf gut barrier assay in anaesthetized, live larvae. Left, control larvae, right, larvae overexpressing *Atg1^{6B}* in the gut enterocytes under control of the *NP1-Gal4* driver. While the distribution of food in the gut of *Atg1^{6B}*-expressing larvae was different from controls, there was no leakage of dye from the gut in any of the animals in three independent experiments (each with $n = 30$ larvae for each genotype).

Data information: Scale bars: A, 20 μm ; B, 1,000 μm .

distribution of DE-cadherin, integrin and MyoII (Fig 9A and B, Appendix Fig S10B). The converse epistatic experiment (upregulating TORC1 signalling while also overexpressing Atg1) also partially suppressed the defects (Appendix Fig S11).

In contrast, a chloroquine block of the last step of autophagy, that is, the fusion of the autophagosomes with lysosomes, resulted

in the expected accumulation of Atg8a-puncta but did not suppress the removal of lateral membrane resulting from TORC1 depletion or Atg1 activation (Appendix Fig S12A–C; compare to Fig 3A–C). Blocking the fusion step by genetic means, that is, by RNAi against Syx17, Vamp7 or Snap29 also did not suppress the defects (Appendix Fig S12D). This shows that the removal of lateral

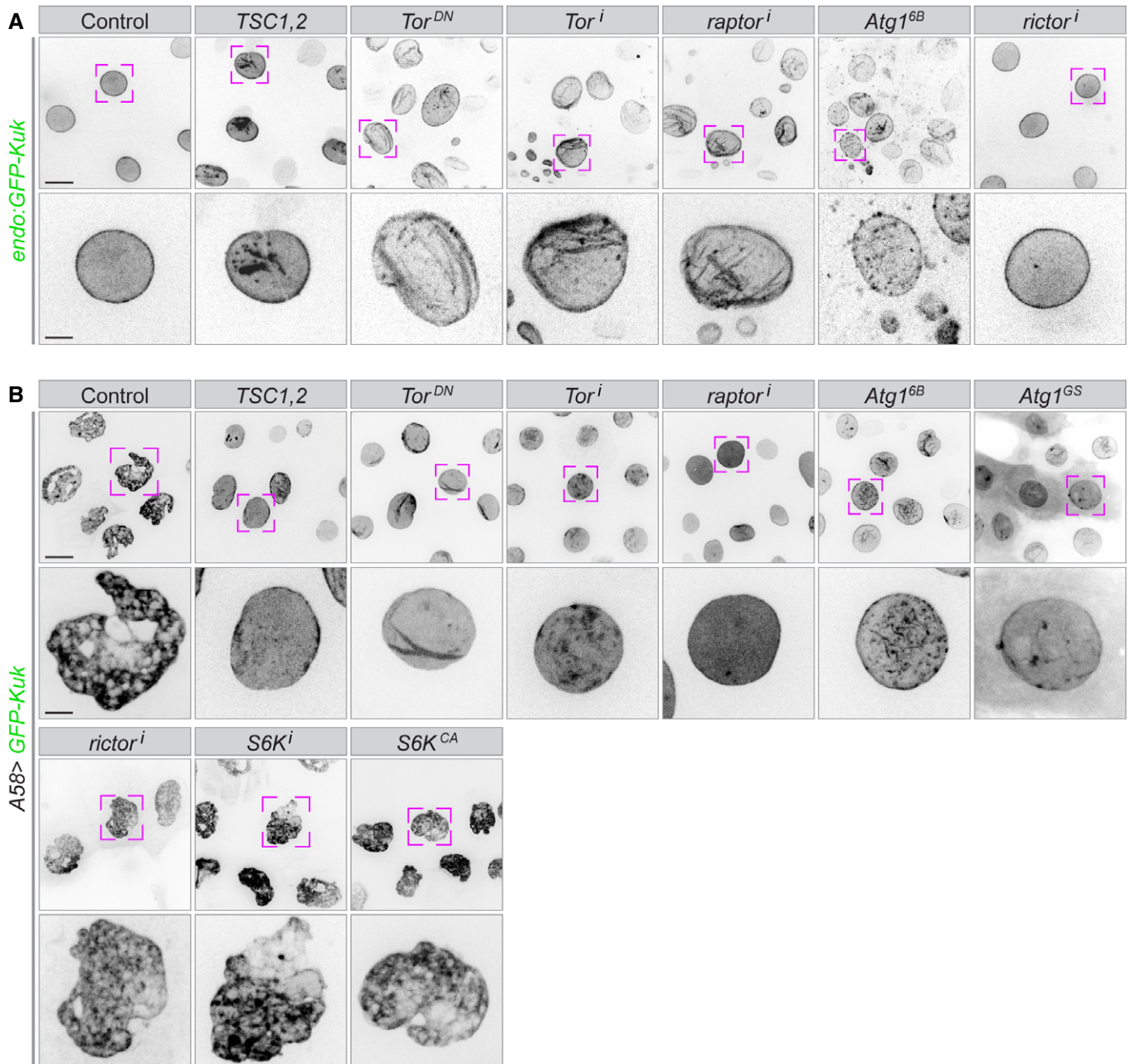


Figure 7. Effect of uncontrolled autophagy on nuclear morphology.

A The nuclear lamina is visualized using a *GFP-tag* inserted into the endogenous locus of the *Kugelkern* (*Kuk*) gene in animals expressing the indicated overexpression or RNAi constructs in the epidermis.

B A GFP-tagged transgenic construct of *Kugelkern* is co-expressed with the indicated overexpression or RNAi constructs. High levels of *Kuk* induce lobulation and other nuclear defects, which are ameliorated if TOR is downregulated or autophagy upregulated, but not if other branches of the TOR signalling pathways (*S6K* or *rictor*) are modified.

Data information: The lower rows show higher magnification of the nuclei marked above. $n = 20\text{--}30$ larvae each genotype. Scale bars: A, B, upper rows, 20 μm ; lower rows, 5 μm .

membrane requires the formation of autophagosomes but not the completion of autophagy, that is, the final degradation of material engulfed by autophagosomes. It also suggests that the lateral plasma membrane material is incorporated into autophagosomes. Staining

with the lipophilic dye BODIPY 493/503 confirmed the strong accumulation of lipids in cytoplasmic vesicles in TORC1-depleted epithelia and other conditions where the lateral membranes were disrupted (Fig 9C and D).

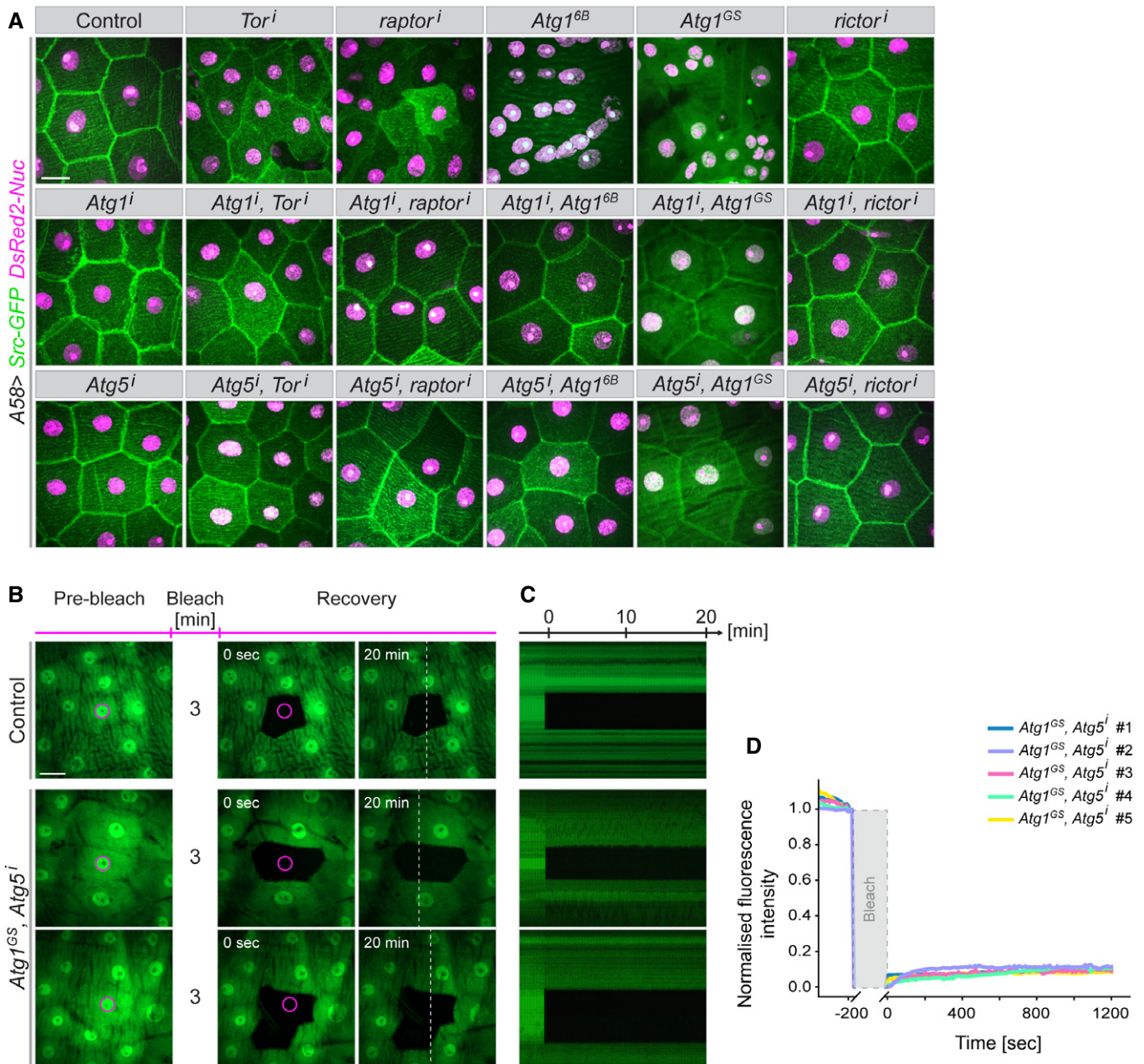


Figure 8. Epistasis of TOR and autophagy.

A The indicated overexpression and RNAi constructs were co-expressed with markers for the plasma membrane (Src-GFP, green) and nuclei (DsRed2-Nuc, magenta) in the larval epidermis. The effects of upregulating autophagy (top row) are suppressed when autophagy is blocked by simultaneously downregulating Atg1 or Atg5. $n = 20$ –40 larvae each genotype.

B–D Atg1-induced syncytium formation is abolished when Atg5 function is downregulated (compare to rows 2 and 3 in Fig 5A and B); same representation as shown in Fig 5A–D.

Data information: Scale bars: A, B, 20 μm . Images from Movie EV17.

Source data are available online for this figure.

The notion that plasma membrane becomes associated with autophagosomes—whether as cargo or as part of the phagophore membrane—is further supported by wound-healing experiments where we co-expressed the trans-membrane markers FasIII-GFP or mCD8-GFP with Atg8a-mCherry. As wound healing progresses and

autophagosomes appear, the markers become increasingly colocalized (Fig 10A and B, Appendix Fig S13A–C and Movies EV18–EV20).

Finally, further evidence for an association of autophagosomes with lateral plasma membrane comes from electron microscopy.

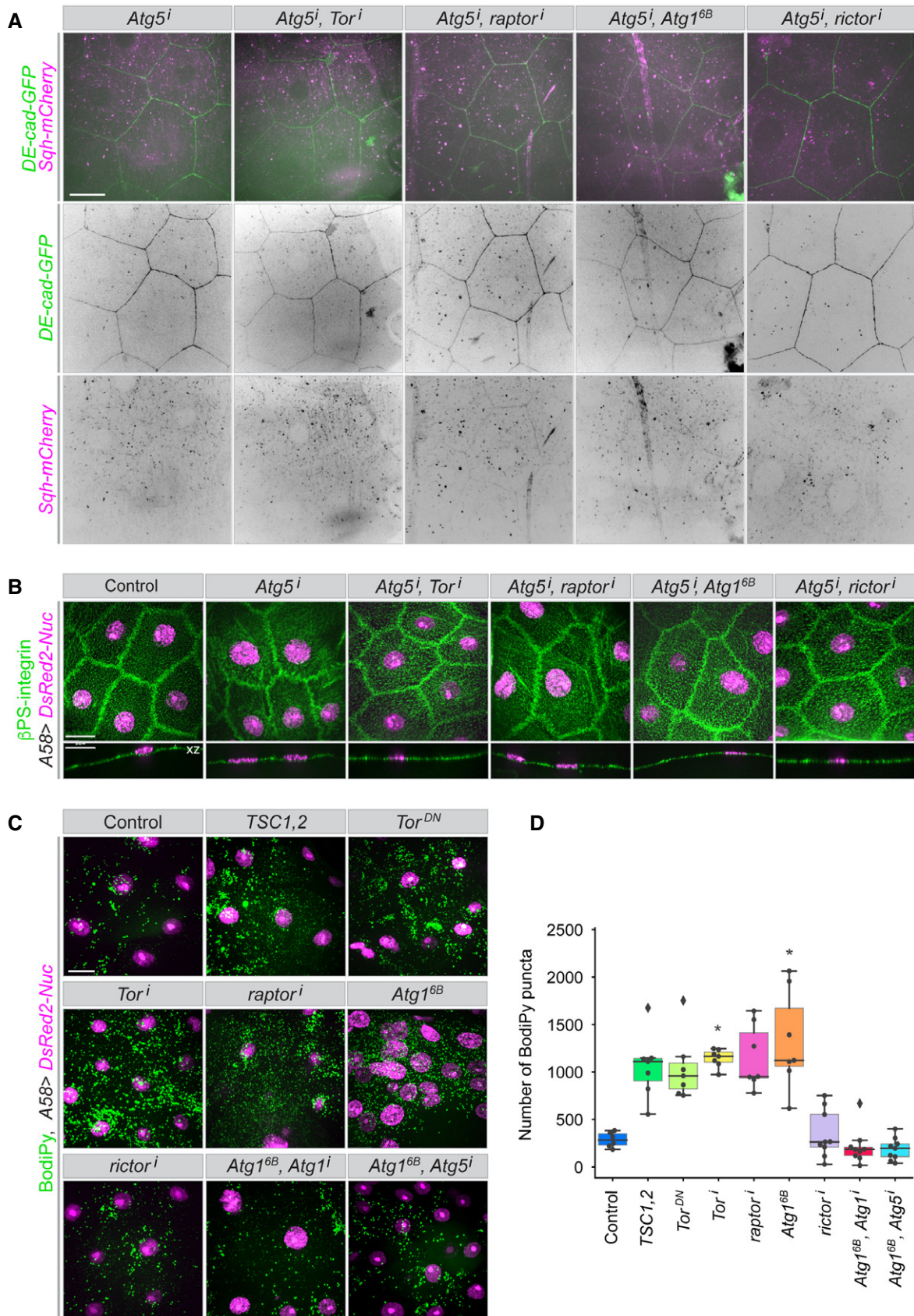


Figure 9.

Figure 9. Dependence of cellular defects on functional autophagy.

A, B Blocking autophagy by downregulating Atg5 suppresses the cellular defects caused by downregulation of TOR signalling: (A) loss of lateral membranes, formation of actin bundles; (B) integrin mislocalization (compare to Fig 4D and E and Appendix Fig S3E and S4C).

C, D Accumulation of neutral lipid in the cytoplasm under conditions of uncontrolled autophagy. (C) Fixed epidermis from larvae expressing the indicated constructs was stained with BodiPy 493/503 to mark lipid accumulations. (D) Quantification of the number of lipid puncta in an epidermal area of 10,000 μm^2 in the indicated conditions. A–D, $n = 7$ –20 larvae each genotype. We assumed unequal sample size and unequal variances and calculations were performed. Values are presented as box plots. Box plot elements are: centre line, median; box limits, upper and lower quartiles; whiskers, 1.5 \times interquartile range; points, outliers. For statistical hypothesis testing, independent and non-parametric (Kruskal–Wallis) t -tests were performed for the mean number of spots in control and experimental conditions. P -values are indicated as follows: * $P < 0.04$ and lack of an asterisk means non-significant ($P > 0.123$).

Data information: Scale bars: 20 μm . Images from Movie EV22.
Source data are available online for this figure.

Autophagosomes are seen in direct contact the plasma membrane, including at sites of cell–cell junctions (Fig 10C).

Activation of autophagy also affected the distribution of actomyosin. We tested whether this was an independent, parallel effect, or part of the mechanism to remodel the plasma membrane. To examine this, we interfered with MyoII activation with a dominant negative version of the MyoII, activator Sqa^{T279A} (“Sqa^{KA}”) or RNAi against *Rok*. These treatments led to the disappearance of the abnormal actomyosin fibres (Tang *et al.*, 2011), but did not suppress the membrane defects (Appendix Figs S14A and B and S2E). Thus, abnormal MyoII activation is not responsible for the autophagy-induced membrane defects.

The fact that elevated Atg1 activity was sufficient to induce the abnormalities suggests that they do not depend on other TORC1-dependent signalling events. We directly tested whether these defects depended on autophagy by reducing Atg1 or Atg5 levels in the background of TORC1 reduction or Atg1 overactivation. This significantly restored wound healing (Appendix Figs S15A and B, Movies EV21 and EV22). In larvae with reduced TORC1 function and lowered Atg1 or Atg5 levels, the actin cables took 16–30 min instead of 40–60 min to form (normal epidermis: 10–12 min) and they were less thick. The total time to complete wound closure was similar as in normal epithelia (120 \pm 20 min, depends on wound size). We had seen above that knockdown of Atg1 is not sufficient to completely suppress the effects of Atg1 overexpression on epithelial cell integrity. Therefore, here too, the remaining defects can probably be ascribed to a remaining slightly elevated level of Atg1 activity, both after TORC1 knockdown and Atg1 upregulation. Atg1 has been observed to affect phosphorylation of the activator, Sqa, and could thereby potentially directly modulate actomyosin in our experiments (Tang *et al.*, 2011). However, the finding that knockdown of Atg5 suppresses the effects on the actomyosin and wound healing shows that the defects do not result from a direct action of Atg1 on myosin but again require the autophagic pathway to occur. They, therefore, seem to be an indirect effect of membrane being sequestered in autophagosomes.

Discussion

Our findings identify: (i) a novel role for the TORC1/autophagy pathway in controlling plasma membrane integrity and homeostasis, (ii) autophagy as a necessary and sufficient inducer of syncytium formation in the epithelium and during wound healing, (iii) wounding as a trigger for autophagy, and (iv) the plasma membrane as potential source for autophagosome formation. On the basis of our observations, we discuss the role of autophagy for syncytium

formation, epithelial barrier function, phagocytosis, actomyosin organization and homeostasis of endomembranes.

Multinucleated cells form during development and ageing or under stress conditions in diverse tissues and organisms by different mechanisms such as cytokinesis failure, entosis, cell–cell fusion or by lateral membrane breaching (Pandit *et al.*, 2013; Moein *et al.*, 2020). We will concentrate only on the latter here, and, in particular, on the connection to autophagy.

A number of studies indicate a correlation between autophagy and syncytium formation. The best studied cases are the fusion of myoblasts during muscle fibre formation and of trophoblast cells during placenta formation (Kim *et al.*, 2015; Fortini *et al.*, 2016). In adult mouse, the stem cells of skeletal muscles (myosatellite cells) are quiescent until external stimuli, such as exercise or injury, trigger their re-entry into the cell cycle and their differentiation to muscle progenitor cells (myoblasts). Myoblasts which have differentiated from adult muscle stem cells after external stimuli, such as exercise or injury, differentiate and fuse to form new multinucleated myofibers. TORC1-dependent autophagy is induced during myogenesis in physiological and pathological conditions such as fasting, atrophy, exercise or injury (Fortini *et al.*, 2016; Fujita *et al.*, 2017). Similar to our observations in the epidermis, inhibition of autophagy in myoblasts *in vitro* interferes with fusion [but not myoblast differentiation], but the mechanism of action for this has not been determined (Fortini *et al.*, 2016).

Trophoblast differentiation represents another example for a potential correlation between autophagy and syncytium formation. The outer trophoblast cells in early mammalian embryos fuse with each other and form a multinucleated syncytiotrophoblast, which later establishes direct contact with the maternal blood that reaches the placental surface. Apart from enabling the exchange of nutrients, the syncytiotrophoblast also provides a barrier against maternal-fetal transmission of pathogens. Autophagy induces in both trophoblast layers, but the highest level of autophagy has been documented in the syncytiotrophoblast during cell fusion (Saito & Nakashima, 2013; Redman *et al.*, 2020). Reduction of autophagy by Atg16L1 knockdown [even after rapamycin treatment] in both human and mouse placenta increases bacterial colonization, but again it is not clear by what mechanism (Saito & Nakashima, 2013; Cao *et al.*, 2016). Extrapolating from our own results, it is possible that also in this system, autophagy and syncytium formation are connected, in that autophagy leads to syncytization and thereby establishes the barrier function of the syncytiotrophoblast.

This leads us to speculate that perhaps in the *Drosophila* epidermis too, syncytium formation during wound healing may serve a protective function. We have seen that autophagy and syncytium

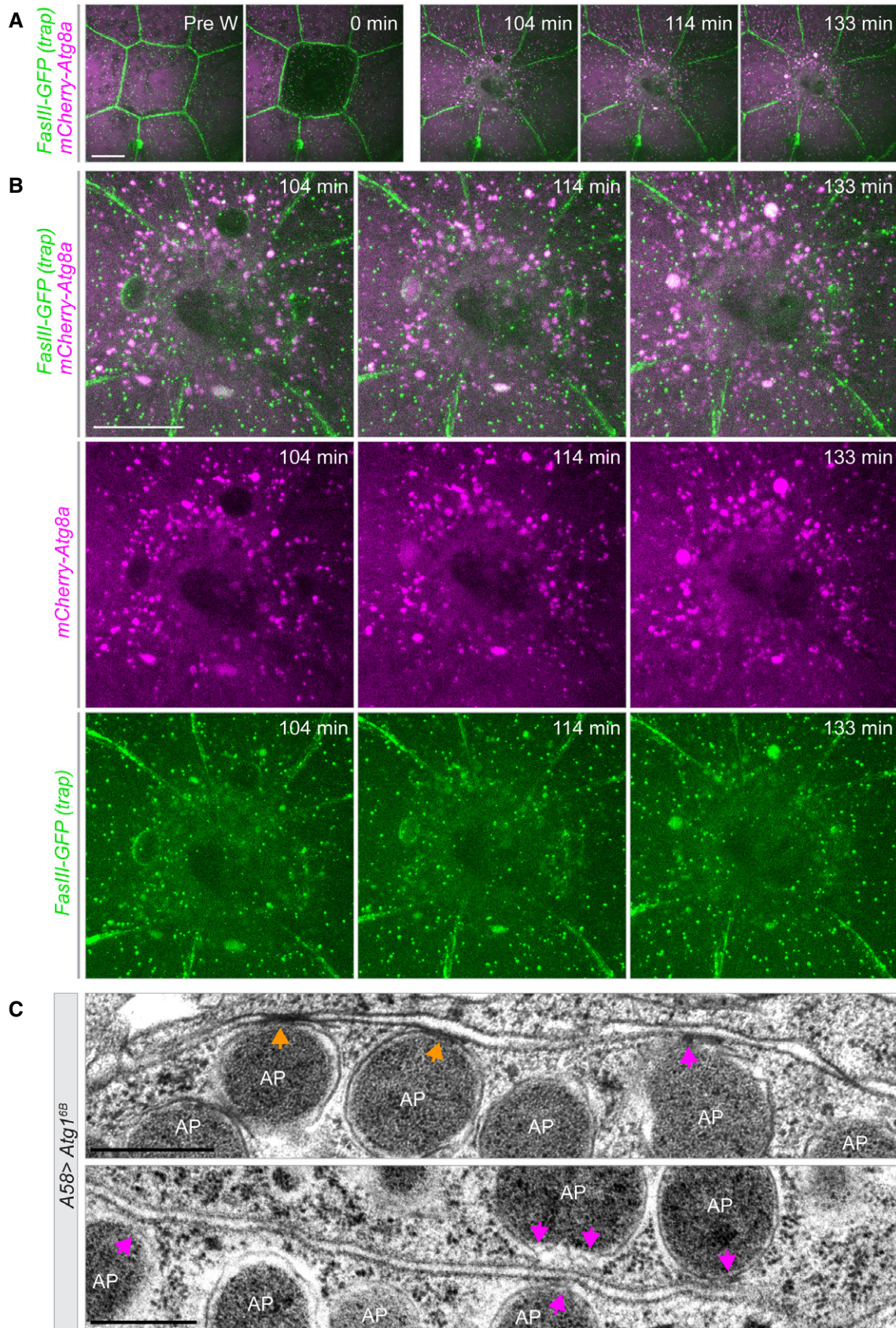


Figure 10.

Figure 10. Colocalization of Atg8a and septate junction component FasIII during epidermal wound healing.

- A, B Time-lapse series of single-cell wound healing in a larva expressing mCherry-Atg8a (magenta) (*A58>mCherry-Atg8a*) and endogenously tagged FasIII (GFP gene trap; green), a transmembrane component of septate junctions. (B) Higher magnification of the post-wounding time points in (A). Images from Movie EV18; see also Movies EV19 and EV20. Each frame is a merge of 68 planes spaced 0.28 μm apart. A, $n = 11$ larvae
- C Transmission electron microscopy of larval epidermis overexpressing Atg16B shows autophagosomes in direct contact with plasma membrane (magenta arrows) and at the sites of cell–cell junctions (orange arrows). The lower panel shows a higher magnification of *Atg1^{6B}* image in Fig 3D.
- Data information: Scale bars: A, B 20 μm ; C 500 nm.

formation are not necessary for wound closure as such, but that autophagy induces events indicative of enhanced barrier formation such as elevated levels of integrin in the apical compartment, a thicker basal lamina and a thicker outer cuticular region (Dong *et al*, 2019). This may reinforce the freshly closed wound and protect it better against the external pathogens, especially in cases where the cuticle was compromised.

Another function of autophagy in the cells surrounding the wound may be to clear up debris. This is also seen in other instances. Autophagy is induced during Planarian regeneration in healthy cells adjacent to the wound and dead cells are phagocytosed by them (Gonzalez-Estevéz *et al*, 2007; Kang *et al*, 2019). The cells surrounding the wounds in our experiments, also engulfed the wound debris (Galko & Krasnow, 2004; Kakanj *et al*, 2016). Whether multinucleated cells phagocytose and digest debris more efficiently (Milde *et al*, 2015) remains to be seen.

Atg1/Ulk can activate myosin and drive autophagosome trafficking both in *Drosophila* and in mammalian cell lines (Tang *et al*, 2011). This may explain the appearance of large cortical and cytosolic actomyosin filaments when autophagy was deregulated. It was perhaps counterintuitive that when the syncytium was wounded, the rate of the formation of the actin cable around the wound and subsequent wound closure were reduced. However, if both autophagy and wound closure need myosin activation, it is conceivable that autophagy might compete for regulators of actin assembly or contractility and thereby slow down actomyosin cable formation and wound closure. We saw that activation of actomyosin is not the cause but the consequence of the lateral membrane disassembly so that plasma membrane defects and wound-healing delay are completely improved when autophagy reduced.

It is becoming clear that besides organelles, such as ER, Golgi or mitochondria, also the plasma membrane can supply the lipids or membrane required for autophagosome formation (Ravikumar *et al*, 2010; Pavel & Rubinsztein, 2017). While we see the large reservoir of lateral membrane being depleted in the epidermis, we do not know whether the material that is removed gives rise to autophagosomal membrane or reaches this compartment as cargo. Some of the components acting in the early steps of autophagosome assembly such as Atg16 and Atg9 are localized at the plasma membrane under normal conditions, where they directly interact with junctional components such as connexin (component of gap junction) and Patj (component of the apical cell polarity complex); they act in the delivery of plasma membrane or lipids to autophagosomes and in a polarized cell could contribute to the identification of the membrane domain to be used for autophagosome assembly (Ravikumar *et al*, 2010; Bejarano *et al*, 2014; Iyyathurai *et al*, 2016; Wen *et al*, 2017; Kiss *et al*, 2020). In the *Drosophila* ovaries, Atg9 is localized on the lateral plasma membrane in nurse cells, and loss of it leads to syncytium formation (Kiss *et al*, 2020). Why

mitochondria are spared in the epidermis, whereas all other organelle membranes are depleted, is not clear.

Finally, in a *Drosophila* pathophysiological model for nuclear laminopathies, the amount of nuclear membrane and its folding are increased (Brandt *et al*, 2006, 2008; Polychronidou *et al*, 2010; Polychronidou & Grobhans, 2011; Petrovsky *et al*, 2018). Overactivation of autophagy improves the morphology and integrity of the nuclear envelope caused by Lamin B or Kugelkern overexpression. In summary, fine tuning of autophagy activity during development and tissue homeostasis is important for plasma membrane integrity.

Materials and Methods

Fly stocks

Fly stocks and crosses were maintained at 25°C under a 12:12 h light/dark cycle at constant 65% humidity on standard fly food. All stocks were in a *white* genetic background. We used the *A58-Gal4* driver line to express UAS-constructs in the epidermis (Galko & Krasnow, 2004) from the end of the first instar onward. Fly stocks are listed in Table 1, fly genotypes in Table 2.

Flip-out experiments

Atg1ⁱ or *Atg5ⁱ* clones in the epidermis were generated with a flip-out system (Pignoni & Zipursky, 1997; Sun & Tower, 1999). Female flies with the genotype *w¹¹¹⁸, hsf1p; act> y⁺>Gal4, UAS-GFP/CyO; +* were crossed with *w¹¹¹⁸, UAS-Atg1ⁱ; ubi:DE-cad-RFP/TM6B* or *w¹¹¹⁸; UAS-Atg5ⁱ; ubi:DE-cad-RFP/TM6B* males or in control experiments with *w¹¹¹⁸; +; ubi:DE-cad-RFP/TM3* males. Clones were identified by GFP expression under the act5C promoter. Mating was carried out at 18°C and at this condition no GFP was detected. The flip-out was induced in mid-stage L2 larvae by heat shock (15 or 30 min in a 37°C *water bath*). The larvae were incubated for 30 h at 25°C followed by wounding and imaging.

Gal80^{ts} experiment

The temperature-sensitive Gal80 system (Gal80^{ts}) was used for time-controlled induction of UAS-constructs (McGuire *et al*, 2003). *w¹¹¹⁸; tub:Gal80^{ts}; A58-Gal4, UAS-Src-GFP, UAS-DsRed2-Nuc/TM6B* females were crossed to males carrying the target UAS constructs at 18°C; at this temperature, no *Src-GFP* was detected. For inactivation of Gal80^{ts}, larvae were heat shocked in a 30°C water bath for 6, 18 or 24 h. Less than 5 h of heat shock was not sufficient to induce the *Src-GFP* marker in the epidermis. Live imaging of larvae with Gal80^{ts} was carried out at 30°C.

Table 1. Fly stocks used in experiments.

Transgenes	Stock ID	Source	Reference
<i>A58-Gal4/TM6B</i>		Michael J. Galko	Galko and Krasnow (2004)
<i>A58-Gal4, UAS-DsRed2-Nuc/TM6B</i>		Michael J. Galko	Galko and Krasnow (2004)
<i>A58-Gal4, UAS-Src-GFP, UAS-DsRed2-Nuc/TM6B</i>		Michael J. Galko	Galko and Krasnow (2004)
<i>NP1-Gal4</i>		Michael Boutros	Jiang et al (2009), Nehme et al (2007)
<i>endo:DE-cad-GFP</i>		Yang Hong	Huang et al (2009)
<i>endo:Sqh-mCherry</i>		Eric F. Wieschaus	Martin et al (2009), Royou et al (2002)
<i>endo:DE-cad-GFP, endo:Sqh-mCherry</i>		Thomas Lecuit	Huang et al (2009), Martin et al (2009)
<i>ubi:DE-cad-RFP/TM3</i>		Hiroki Oda	Oda and Tsukita (2001)
<i>FasIII-GFP (GFP-trap) (FasIII-GFP[G00258])</i>	BL # 50841	Michael J. Galko	Morin et al (2001)
<i>Nrg-GFP (GFP-trap) (Nrg-GFP[G00305])</i>	BL # 6844	Michael J. Galko	Morin et al (2001)
<i>Klaroid-GFP (GFP-exon-Trap) (koi-GFP[CB04483])</i>	BL # 51525	Allan C. Spradling	Buszczak et al (2007)
<i>endo:GFP-Kuk</i>		Jörg Großhans	Polychronidou et al (2010)
<i>UAS-GFP-Kuk (UAS-GFP-Kuk^{EY07696(w⁺)})</i>		Jörg Großhans	Polychronidou et al (2010)
<i>UAS-RFP-LamB (UASp-mRFP-LaminDm0^{19(w⁺)})</i>		Jörg Großhans	Polychronidou et al (2010)
<i>endo:His2AV-mRFP1</i>		Stefan Heidmann	Schuh et al (2007)
<i>UASp-GalT-GFP</i>	BL # 31422	Jennifer Lippincott-Schwartz	Cole et al (1996)
<i>UASp-KDEL.RFP</i>	BL # 30910	Jennifer Lippincott-Schwartz	Cole et al (1996)
<i>UAS-GFP (UAS-EGFP)</i>	BL # 5431	Eric Spana	FBrf0217672
<i>UAS-mito-GFP</i>	BL # 8442	Allan C. Spradling	Cox and Spradling (2003)
<i>UAS-mCDS-GFP</i>	BL # 5137	Liqun Luo	Lee and Luo (1999)
<i>UAS-GFP-Atg8a</i>		Thomas P. Neufeld	Arsham and Neufeld (2009)
<i>UAS-mCherry-Atg8a</i>	BL # 37750	Ioannis Nezis	FBrf0111645
<i>UAS-LAMP1-GFP</i>		Gábor Juhász	Takats et al (2013)
<i>UAS-GFP-Baz</i>		Daniel St Johnston	Benton and St Johnston (2003)
<i>UAS-GFP-Dlg (UAS-EGFP-Dlg-S97)</i>		Ulrich Thomas	Bachmann et al (2004)
<i>UAS-Atg1ⁱ (UAS-Atg1^{RNAi})</i>	V # 16133 (GD7149)	Barry J. Dickson	Dietzl et al (2007)
<i>UAS-Atg5ⁱ (UAS-Atg5^{RNAi})</i>	V # 104461 (KK108904)	Barry J. Dickson	Dietzl et al (2007)
<i>UAS-Atg6ⁱ (UAS-Atg6^{RNAi})</i>	V # 110197 (KK102460)	Barry J. Dickson	(Dietzl et al, 2007)
<i>UAS-Atg7ⁱ (UAS-Atg7^{RNAi})</i>	V # 45558 (GD11671)	Barry J. Dickson	Dietzl et al (2007)
<i>UAS-Atg12ⁱ (UAS-Atg12^{RNAi})</i>	V # 29791 (GD15230)	Barry J. Dickson	Dietzl et al (2007)
<i>UAS-TSC1,2 (UAS-TSC1, AUS-TSC2)</i>		Iswar K. Hariharan	Tapon et al (2001)
<i>UAS-TSC1ⁱ (UAS-TSC1^{RNAi})</i>	V # 22252 (GD11836)	Barry J. Dickson	Dietzl et al (2007)
<i>UAS-TSC1ⁱ⁻² (UAS-TSC1^{RNAi})</i>	BL # 54043	Robert Perrimon	Perkins et al (2015)
<i>UAS-Torⁱ (UAS-Tor^{RNAi})</i>	BL # 33951	Robert Perrimon	Perkins et al (2015)
<i>UAS-TOR^{DN} (UAS-TOR^{TED})</i>	BL # 7013	Thomas P. Neufeld	Hennig and Neufeld (2002)
<i>UAS-raptorⁱ (UAS-raptor^{RNAi})</i>	BL # 34814	Robert Perrimon	Perkins et al (2015)
<i>UAS-raptorⁱ⁻² (UAS-raptor^{RNAi})</i>	BL # 41912	Robert Perrimon	Perkins et al (2015)
<i>UAS-rictorⁱ (UAS-rictor^{RNAi})</i>	BL # 36699	Robert Perrimon	Perkins et al (2015)
<i>UAS-Atg1^{6B} (UAS-Atg1^{6B})</i>		Thomas P. Neufeld	Scott et al (2007)
<i>UAS-Atg1^{CS}, UAS-GFP (UAS-Atg1^{CS10797})</i> In this line, UAS regulatory sequence have been inserted upstream of the endogenous Atg1 gene		Thomas P. Neufeld	Scott et al (2007)
<i>UAS- AMPK^{CA} (UAS- AMPK^{T184D})</i>	BL # 32110	Jay Brenman	FBrf0211859
<i>UAS-S6Kⁱ (UAS-S6K^{RNAi})</i>	BL # 41895	Robert Perrimon	Perkins et al (2015)
<i>UAS-S6K^{CA} (UAS-S6K^{STDETE})</i>	BL # 6914	Mary Stewart	Barcelo and Stewart (2002)
<i>UAS-Sqa^{KA} (UAS-Sqa^{T279A}/CyO)</i>		Guang-Chao Chen	Tang et al (2011)

Table 1 (continued)

Transgenes	Stock ID	Source	Reference
<i>UAS-RhoAⁱ</i> (<i>UAS-RhoA^{RNAi}</i>)	V # 12734 (GD4726)	Barry J. Dickson	Dietzl et al (2007)
<i>UAS-RoKⁱ</i> (<i>UAS-RoK^{RNAi}</i>)	V # 104675 (KK107802)	Barry J. Dickson	Dietzl et al (2007)
<i>UAS-Rheb^{AV4}</i>		Fuyuhiko Tamanoi	Patel et al (2003)
<i>UAS-Syx17ⁱ</i> (<i>UAS-Syx17^{RNAi}</i>)	V # 36595 (GD14850)	Barry J. Dickson	Dietzl et al (2007)
<i>UAS-Vamp7ⁱ</i> (<i>UAS-Vamp7^{RNAi}</i>)	BL # 38300	Robert Perrimon	Perkins et al (2015)
<i>UAS-Snap29ⁱ</i> (<i>UAS-Snap29^{RNAi}</i>)	V # 18172 (GD7222)	Barry J. Dickson	Dietzl et al (2007)
<i>UAS-Snap29^j</i> (<i>UAS-Snap29^{RNAi}</i>)	V # 107947 (KK108034)	Barry J. Dickson	Dietzl et al (2007)
<i>tubP-GAL80^{ES}</i>	BL # 7019	Roland Davis	McGuire et al (2003) FBrf0159874
<i>hsFLP; act5c > y⁺ > GAL4, UAS-GFP/CyO</i>		Konrad Basler	Struhl and Basler (1993)

BL: Bloomington stock centre (<https://bdsc.indiana.edu/>); V: VDRC stock centre (<https://stockcenter.vdrc.at/control/main>).

Chloroquine treatment

Mid-L2 Larvae were transferred to fresh medium containing 3 mg/ml chloroquine (Sigma-Aldrich Cat. # C6628) and 0.3% Erioglaucine disodium (Sigma-Aldrich Cat. # 861146; food colouring to monitor food uptake) for 14 h before imaging.

Smurf gut barrier assay

Female flies with the genotype *w¹¹¹⁸; NPI-Gal4; +* were crossed with *w¹¹¹⁸; +; UAS-Atg1^{6B}* males or, in control experiments (Rera et al, 2012), with *w¹¹¹⁸; +; +* males. The progeny was raised on standard fly food containing 0.3% Erioglaucine disodium (Sigma-Aldrich Cat. # 861146) at 25°C. For the Smurf assay, L3 larvae were anaesthetized with ether (Kakanj et al, 2020) and analysed and recorded on an AxioZoom.V16 microscope (Zeiss).

Immunostaining

For immunofluorescent staining, L3 larvae were dissected in phosphate-buffered saline (PBS), fixed in 4% formaldehyde or 4% paraformaldehyde for 30 min at room temperature (RT) and blocked in 1% BSA and 0.3% Triton-X for 2 h at RT. Primary and secondary antibodies were incubated for 2 h at RT. The tissues were mounted with Fluoromount-G for confocal imaging. Antiserum dilutions and sources: Bazooka (1:500, from A. Wodarz), a-PKC (1:500, Santa Cruze, ID-Nr #406), FasIII (1:2,000, DSHB, #7G10), β PS-integrin (1:200, DSHB #CF.6G11), anti-rabbit or anti-mouse immunoglobulin-G labelled with Alexa 488 (1:200; Invitrogen). BodiPy 493/503 (ThermoFisher Cat. #D3922) was used at 1: 500. To image the gut (Fig 6A), male flies with the genotype *w¹¹¹⁸; NPI-Gal4/+; UAS-GFP-Dlg/+* were crossed with *w¹¹¹⁸; +; UAS-Atg1^{6B}* females or, in control experiments, with *w¹¹¹⁸; +; +* females. The guts were isolated from unstarved larvae, fixed and mounted in 4% paraformaldehyde and directly imaged.

FLIP procedures

A modified FLIP procedure (DeLotto et al, 2007) was applied to the dorsal larval epidermis in the abdominal segments A3–A5 of L3 instar larvae on an inverted spinning disk microscope equipped with FRAPPA and a 40 \times /1.3 oil objective lens (see section Microscope setup). 7–19 frames were acquired before bleaching. 16-bit depth images were taken

at a magnification of 0.163 μ m/pixel acquiring a z-stack of 2.1 μ m. Photobleaching (one bleaching event per cell, mid-cytosolic plane) was performed using 100% laser power over 3 or 20 min.

Immobilizing larvae

Early L3 larvae were anaesthetized with diethyl ether (Kakanj et al, 2020).

Laser ablation

All laser ablations and wounding experiments were performed exactly as described previously (Kakanj et al, 2020). For single-cell wounds, the nucleus was targeted with 1 pulse/ μ m UV laser power of \sim 0.30 μ J energy (measured on the objective lens). For laser cuts at the plane of the apical plasma membrane without inducing a wound-healing response, the UV laser was set to 1 pulse/ μ m of \sim 0.25 μ J energy.

Microscope setup and live imaging

We used an inverted spinning disk confocal microscope (Nikon TiE model with Yokogawa, model no. CSU-X1 system) with a nano-positioning Piezo Z stage control system (NanoScan, model no. OP400, Prior Scientific), Plan-Fluor 40 \times /1.3 numerical aperture (NA) oil-immersion differential interference contrast (DIC) objective or Plan-Apochromat 60 \times /1.2 NA water-immersion objective; EMCCD camera (CamLink, model no. C9100-50; 1,000 \times 1,000 pixels) controlled by Volocity v.6.3.57, with 488-nm and 561-nm channels. z-stacks were taken with a step size of 0.28 μ m with 60 \times /1.2 and 0.24 μ m with 40 \times /1.3 (45–95 z-stacks, covering a 10–30- μ m depth) both for live and fixed specimens (Kakanj et al, 2020). All figures and videos show merged z-stacks. After live imaging, larvae were returned individually into food vials and monitored for survival. We evaluated data only from larvae that survived at least 2 days post imaging. Live imaging used for all images shown in this paper, except electron micrographs and images in Figs 4E, 6A and 9B and C, Appendix Figs S3A–C and S4C, which are from fixed specimens.

Image processing

For image processing we used Volocity v.6.3.57 (PerkinElmer) or Fiji (National Institutes of Health).

Table 2. List of genotypes used in experiments.

Figure no. or Movie no.	Fly stock/cross
1 A, B, C, D	<i>w¹¹¹⁸</i> ; <i>UAS-GFP-Atg8a/+</i> ; <i>A58-Gal4/+</i> (Control)
1 A, B, D	<i>w¹¹¹⁸</i> ; <i>UAS-GFP-Atg8a/UAS-Atg1ⁱ</i> ; <i>A58-Gal4/+</i>
1 A, B, D	<i>w¹¹¹⁸</i> ; <i>UAS-GFP-Atg8a/UAS-Atg5ⁱ</i> ; <i>A58-Gal4/+</i>
1 A, B, D	<i>w¹¹¹⁸</i> ; <i>UAS-GFP-Atg8a/UAS-Atg6ⁱ</i> ; <i>A58-Gal4/+</i>
1 D	<i>w¹¹¹⁸</i> ; <i>UAS-GFP-Atg8a/+</i> ; <i>A58-Gal4/UAS-Atg7^j</i>
1 D	<i>w¹¹¹⁸</i> ; <i>UAS-GFP-Atg8a/+</i> ; <i>A58-Gal4/UAS-Atg12^j</i>
1 D	<i>w¹¹¹⁸</i> ; <i>UAS-GFP-Atg8a/+</i> ; <i>A58-Gal4/UAS-TSC1ⁱ</i>
1 D	<i>w¹¹¹⁸</i> ; <i>UAS-GFP-Atg8a/UAS-Rheb^{AV4}</i> ; <i>A58-Gal4/+</i>
1 E	<i>w¹¹¹⁸</i> ; +; <i>A58-Gal4</i> , <i>UAS-Src-GFP</i> , <i>UAS-DsRed2-Nuc/+</i> (Control)
1 E	<i>w¹¹¹⁸</i> ; <i>UAS-Atg1ⁱ/+</i> ; <i>A58-Gal4</i> , <i>UAS-Src-GFP</i> , <i>UAS-DsRed2-Nuc/+</i>
1 E	<i>w¹¹¹⁸</i> ; <i>UAS-Atg5ⁱ/+</i> ; <i>A58-Gal4</i> , <i>UAS-Src-GFP</i> , <i>UAS-DsRed2-Nuc/+</i>
1 F	<i>w¹¹¹⁸</i> ; <i>endo:DE-Cad-GFP</i> , <i>endo:Sqh-mCherry/+</i> ; <i>A58-Gal4/+</i> (Control)
1 F	<i>w¹¹¹⁸</i> ; <i>endo:DE-Cad-GFP</i> , <i>endo:Sqh-mCherry/UAS-Atg1ⁱ</i> ; <i>A58-Gal4/+</i>
1 F	<i>w¹¹¹⁸</i> ; <i>endo:DE-Cad-GFP</i> , <i>endo:Sqh-mCherry/UAS-Atg5ⁱ</i> ; <i>A58-Gal4/+</i>
2 B, C, D	<i>w¹¹¹⁸</i> , <i>hsflp/+</i> ; <i>act5c > y⁺ > Gal4</i> , <i>UAS-GFP/+</i> ; <i>ubi:DE-cad-RFP/+</i> (Control)
2 B	<i>w¹¹¹⁸</i> , <i>hsflp/+</i> ; <i>act5c > y⁺ > Gal4</i> , <i>UAS-GFP/UAS-Atg1ⁱ</i> ; <i>ubi:DE-cad-RFP/+</i>
2 B	<i>w¹¹¹⁸</i> , <i>hsflp/+</i> ; <i>act5c > y⁺ > Gal4</i> , <i>UAS-GFP/UAS-Atg5ⁱ</i> ; <i>ubi:DE-cad-RFP/+</i>
3 A, B, C	<i>w¹¹¹⁸</i> ; <i>UAS-GFP-Atg8a/+</i> ; <i>A58-Gal4/+</i> (Control)
3 A, B, C	<i>w¹¹¹⁸</i> ; <i>UAS-GFP-Atg8a/UAS-AMPKα^{CA}</i> ; <i>A58-Gal4/+</i>
3 A, B, C	<i>w¹¹¹⁸</i> ; <i>UAS-GFP-Atg8a/+</i> ; <i>A58-Gal4/UAS-Tor^j</i>
3 A, B, C	<i>w¹¹¹⁸</i> ; <i>UAS-GFP-Atg8a/+</i> ; <i>A58-Gal4/UAS-raptor^j</i>
3 A, B, C	<i>w¹¹¹⁸</i> ; <i>UAS-GFP-Atg8a/+</i> ; <i>A58-Gal4/UAS-Atg1^{6B}</i>
3 A, B, C	<i>w¹¹¹⁸</i> ; <i>UAS-GFP-Atg8a/+</i> ; <i>A58-Gal4/UAS-ric1^j</i>
3 A, B, C	<i>w¹¹¹⁸</i> ; <i>UAS-GFP-Atg8a/+</i> ; <i>A58-Gal4/UAS-TSC1ⁱ</i>
3 C	<i>w¹¹¹⁸</i> ; <i>UAS-GFP-Atg8a/UAS-TSC1</i> , <i>UAS-TSC2</i> ; <i>A58-Gal4/+</i>
3 C	<i>w¹¹¹⁸</i> ; <i>UAS-GFP-Atg8a/UAS-Tor^{DN}</i> ; <i>A58-Gal4/+</i>
3 C	<i>w¹¹¹⁸</i> ; <i>UAS-GFP-Atg8a/UAS-raptor^{j-2}</i> ; <i>A58-Gal4/+</i>
3 C	<i>w¹¹¹⁸</i> ; <i>UAS-GFP-Atg8a/UAS-Rheb^{AV4}</i> ; <i>A58-Gal4/+</i>
3 D, E, F	<i>w¹¹¹⁸</i> ; +; <i>A58-Gal4</i> , <i>UAS-Src-GFP</i> , <i>UAS-DsRed2-Nuc/+</i> (Control)
3 D, E, F	<i>w¹¹¹⁸</i> ; +; <i>A58-Gal4</i> , <i>UAS-Src-GFP</i> , <i>UAS-DsRed2-Nuc/UAS-raptor^j</i>
3 D, E	<i>w¹¹¹⁸</i> ; +; <i>A58-Gal4</i> , <i>UAS-Src-GFP</i> , <i>UAS-DsRed2-Nuc/UAS-Atg1^{GS}</i> , <i>UAS-GFP</i>
3 D, E, F	<i>w¹¹¹⁸</i> ; +; <i>A58-Gal4</i> , <i>UAS-Src-GFP</i> , <i>UAS-DsRed2-Nuc/UAS-Atg1^{6B}</i>
3 F	<i>w¹¹¹⁸</i> ; <i>UAS-AMPKα^{CA}/+</i> ; <i>A58-Gal4</i> , <i>UAS-Src-GFP</i> , <i>UAS-DsRed2-Nuc/+</i>
3 F	<i>w¹¹¹⁸</i> ; <i>UAS-TSC1</i> , <i>UAS-TSC2/+</i> ; <i>A58-Gal4</i> , <i>UAS-Src-GFP</i> , <i>UAS-DsRed2-Nuc/+</i>

Table 2 (continued)

Figure no. or Movie no.	Fly stock/cross
3 F	<i>w¹¹¹⁸</i> ; +; <i>A58-Gal4</i> , <i>UAS-Src-GFP</i> , <i>UAS-DsRed2-Nuc/UAS-Tor^j</i>
3 F	<i>w¹¹¹⁸</i> ; +; <i>A58-Gal4</i> , <i>UAS-Src-GFP</i> , <i>UAS-DsRed2-Nuc/UAS-ric1^j</i>
3 H	<i>w¹¹¹⁸</i> ; <i>tub:Gal80^{TS/+}</i> ; <i>A58-Gal4</i> , <i>UAS-Src-GFP</i> , <i>UAS-DsRed2-Nuc/UAS-Atg1^{6B}</i>
4 A	<i>w¹¹¹⁸</i> ; <i>UAS-GFP-Baz/+</i> ; <i>A58-Gal4/+</i> (Control)
4 A	<i>w¹¹¹⁸</i> ; <i>UAS-GFP-Baz/UAS-TSC1</i> , <i>UAS-TSC2</i> ; <i>A58-Gal4/+</i>
4 A	<i>w¹¹¹⁸</i> ; <i>UAS-GFP-Baz/UAS-Tor^{DN}</i> ; <i>A58-Gal4/+</i>
4 A	<i>w¹¹¹⁸</i> ; <i>UAS-GFP-Baz/+</i> ; <i>A58-Gal4/UAS-Tor^j</i>
4 A	<i>w¹¹¹⁸</i> ; <i>UAS-GFP-Baz/+</i> ; <i>A58-Gal4/UAS-raptor^j</i>
4 A	<i>w¹¹¹⁸</i> ; <i>UAS-GFP-Baz/+</i> ; <i>A58-Gal4/UAS-Atg1^{6B}</i>
4 A	<i>w¹¹¹⁸</i> ; <i>UAS-GFP-Baz/+</i> ; <i>A58-Gal4/UAS-ric1^j</i>
4 B	<i>w¹¹¹⁸</i> ; <i>endo:FasIII-GFP/+</i> ; <i>A58-Gal4/+</i> (Control)
4 B	<i>w¹¹¹⁸</i> ; <i>endo:FasIII-GFP/UAS-Tor^{DN}</i> ; <i>A58-Gal4/+</i>
4 B	<i>w¹¹¹⁸</i> ; <i>endo:FasIII-GFP/+</i> ; <i>A58-Gal4/UAS-Tor^j</i>
4 B	<i>w¹¹¹⁸</i> ; <i>endo:FasIII-GFP/+</i> ; <i>A58-Gal4/UAS-Atg1^{6B}</i>
4 C	<i>w¹¹¹⁸</i> ; <i>endo:Nrg-GFP/+</i> ; <i>A58-Gal4/+</i> (Control)
4 C	<i>w¹¹¹⁸</i> ; <i>endo:Nrg-GFP</i> ; <i>UAS-Tor^{DN/+}</i> ; <i>A58-Gal4/+</i>
4 C	<i>w¹¹¹⁸</i> ; <i>endo:Nrg-GFP/+</i> ; <i>A58-Gal4/UAS-Atg1^{6B}</i>
4 D	<i>w¹¹¹⁸</i> ; <i>endo:DE-cad-GFP</i> , <i>endo:Sqh-mCherry/+</i> ; <i>A58-Gal4/+</i> (Control)
4 D	<i>w¹¹¹⁸</i> ; <i>endo:DE-cad-GFP</i> , <i>endo:Sqh-mCherry/UAS-TSC1</i> , <i>UAS-TSC2</i> ; <i>A58-Gal4/+</i>
4 D	<i>w¹¹¹⁸</i> ; <i>endo:DE-cad-GFP</i> , <i>endo:Sqh-mCherry/UAS-Tor^{DN}</i> ; <i>A58-Gal4/+</i>
4 D	<i>w¹¹¹⁸</i> ; <i>endo:DE-cad-GFP</i> , <i>endo:Sqh-mCherry/+</i> ; <i>A58-Gal4/UAS-raptor^j</i>
4 D	<i>w¹¹¹⁸</i> ; <i>endo:DE-cad-GFP</i> , <i>endo:Sqh-mCherry/+</i> ; <i>A58-Gal4/UAS-Atg1^{GS}</i> , <i>UAS-GFP</i>
4 D	<i>w¹¹¹⁸</i> ; <i>endo:DE-cad-GFP</i> , <i>endo:Sqh-mCherry/+</i> ; <i>A58-Gal4/UAS-Atg1^{6B}</i>
4 D	<i>w¹¹¹⁸</i> ; <i>endo:DE-cad-GFP</i> , <i>endo:Sqh-mCherry/+</i> ; <i>A58-Gal4/UAS-ric1^j</i>
4 E	<i>w¹¹¹⁸</i> ; +; <i>A58-Gal4</i> , <i>UAS-DsRed2-Nuc/+</i> (Control)
4 E	<i>w¹¹¹⁸</i> ; +; <i>A58-Gal4</i> , <i>UAS-DsRed2-Nuc/UAS-Tor^j</i>
4 E	<i>w¹¹¹⁸</i> ; +; <i>A58-Gal4</i> , <i>UAS-DsRed2-Nuc/UAS-raptor^j</i>
4 E	<i>w¹¹¹⁸</i> ; +; <i>A58-Gal4</i> , <i>UAS-DsRed2-Nuc/UAS-Atg1^{6B}</i>
4 E	<i>w¹¹¹⁸</i> ; +; <i>A58-Gal4</i> , <i>UAS-DsRed2-Nuc/UAS-ric1^j</i>
4 F	<i>w¹¹¹⁸</i> ; +; <i>A58-Gal4</i> , <i>UAS-Src-GFP</i> , <i>UAS-DsRed2-Nuc/+</i> (Control)
5 A, B, C	<i>w¹¹¹⁸</i> ; <i>UAS-GFP/+</i> ; <i>A58-Gal4/+</i> (Control)
5 A, B, C, D	<i>w¹¹¹⁸</i> ; +; <i>A58-Gal4/UAS-Atg1^{GS}</i> , <i>UAS-GFP</i>
5 E, F	<i>w¹¹¹⁸</i> ; +; <i>A58-Gal4</i> , <i>UAS-Src-GFP</i> , <i>UAS-DsRed2-Nuc/+</i> (Control)
5 E, F	<i>w¹¹¹⁸</i> ; +; <i>A58-Gal4</i> , <i>UAS-Src-GFP</i> , <i>UAS-DsRed2-Nuc/UAS-Atg1^{GS}</i> , <i>UAS-GFP</i>
5 E, F	<i>w¹¹¹⁸</i> ; +; <i>A58-Gal4</i> , <i>UAS-Src-GFP</i> , <i>UAS-DsRed2-Nuc/UAS-Atg1^{6B}</i>

Table 2 (continued)

Figure no. or Movie no.	Fly stock/cross
6 A	<i>w</i> ¹¹¹⁸ ; <i>NP1-Gal4/+</i> ; <i>UAS-GFP-Dlg/+</i>
6 A	<i>w</i> ¹¹¹⁸ ; <i>NP1-Gal4/+</i> ; <i>UAS-GFP-Dlg/UAS-Atg1^{6B}</i>
6 B	<i>w</i> ¹¹¹⁸ ; <i>NP1-Gal4/+</i> ; +
6 B	<i>w</i> ¹¹¹⁸ ; <i>NP1-Gal4/+</i> ; <i>UAS-Atg1^{6B}/+</i>
7 A	<i>w</i> ¹¹¹⁸ ; <i>endo:GFP-Kuk/+</i> ; <i>A58-Gal4/+</i> (Control)
7 A	<i>w</i> ¹¹¹⁸ ; <i>endo:GFP-Kuk/UAS-TSC1</i> , <i>UAS-TSC2</i> ; <i>A58-Gal4/+</i>
7 A	<i>w</i> ¹¹¹⁸ ; <i>endo:GFP-Kuk/UAS-Tor^{DN}</i> ; <i>A58-Gal4/+</i>
7 A	<i>w</i> ¹¹¹⁸ ; <i>endo:GFP-Kuk/+</i> ; <i>A58-Gal4/UAS-Tor^J</i>
7 A	<i>w</i> ¹¹¹⁸ ; <i>endo:GFP-Kuk/+</i> ; <i>A58-Gal4/UAS-raptor^J</i>
7 A	<i>w</i> ¹¹¹⁸ ; <i>endo:GFP-Kuk/+</i> ; <i>A58-Gal4/UAS-Atg1^{6B}</i>
7 A	<i>w</i> ¹¹¹⁸ ; <i>endo:GFP-Kuk/+</i> ; <i>A58-Gal4/UAS-rictor^J</i>
7 B	<i>w</i> ¹¹¹⁸ ; <i>UAS-GFP-Kuk/+</i> ; <i>A58-Gal4/+</i> (Control)
7 B	<i>w</i> ¹¹¹⁸ ; <i>UAS-GFP-Kuk/UAS-TSC1</i> , <i>UAS-TSC2</i> ; <i>A58-Gal4/+</i>
7 B	<i>w</i> ¹¹¹⁸ ; <i>UAS-GFP-Kuk/UAS-Tor^{DN}</i> ; <i>A58-Gal4/+</i>
7 B	<i>w</i> ¹¹¹⁸ ; <i>UAS-GFP-Kuk/+</i> ; <i>A58-Gal4/UAS-Tor^J</i>
7 B	<i>w</i> ¹¹¹⁸ ; <i>UAS-GFP-Kuk/+</i> ; <i>A58-Gal4/UAS-raptor^J</i>
7 B	<i>w</i> ¹¹¹⁸ ; <i>UAS-GFP-Kuk/+</i> ; <i>A58-Gal4/UAS-Atg1^{GS}</i> , <i>UAS-GFP</i>
7 B	<i>w</i> ¹¹¹⁸ ; <i>UAS-GFP-Kuk/+</i> ; <i>A58-Gal4/UAS-Atg1^{6B}</i>
7 B	<i>w</i> ¹¹¹⁸ ; <i>UAS-GFP-Kuk/+</i> ; <i>A58-Gal4/UAS-rictor^J</i>
7 B	<i>w</i> ¹¹¹⁸ ; <i>UAS-GFP-Kuk/+</i> ; <i>A58-Gal4/UAS-S6K^I</i>
7 B	<i>w</i> ¹¹¹⁸ ; <i>UAS-GFP-Kuk/+</i> ; <i>A58-Gal4/UAS-S6K^{CA}</i>
8 A	<i>w</i> ¹¹¹⁸ ; +; <i>A58-Gal4</i> , <i>UAS-Src-GFP</i> , <i>UAS-DsRed2-Nuc/+</i> (Control)
8 A	<i>w</i> ¹¹¹⁸ ; +; <i>A58-Gal4</i> , <i>UAS-Src-GFP</i> , <i>UAS-DsRed2-Nuc/UAS-Tor^J</i>
8 A	<i>w</i> ¹¹¹⁸ ; +; <i>A58-Gal4</i> , <i>UAS-Src-GFP</i> , <i>UAS-DsRed2-Nuc/UAS-raptor^J</i>
8 A	<i>w</i> ¹¹¹⁸ ; +; <i>A58-Gal4</i> , <i>UAS-Src-GFP</i> , <i>UAS-DsRed2-Nuc/UAS-Atg1^{6B}</i>
8 A	<i>w</i> ¹¹¹⁸ ; +; <i>A58-Gal4</i> , <i>UAS-Src-GFP</i> , <i>UAS-DsRed2-Nuc/UAS-rictor^J</i>
8 A	<i>w</i> ¹¹¹⁸ ; <i>UAS-Atg1^I/+</i> ; <i>A58-Gal4</i> , <i>UAS-Src-GFP</i> , <i>UAS-DsRed2-Nuc/+</i>
8 A	<i>w</i> ¹¹¹⁸ ; <i>UAS-Atg1^I/+</i> ; <i>A58-Gal4</i> , <i>UAS-Src-GFP</i> , <i>UAS-DsRed2-Nuc/UAS-Tor^J</i>
8 A	<i>w</i> ¹¹¹⁸ ; <i>UAS-Atg1^I/+</i> ; <i>A58-Gal4</i> , <i>UAS-Src-GFP</i> , <i>UAS-DsRed2-Nuc/UAS-raptor^J</i>
8 A	<i>w</i> ¹¹¹⁸ ; <i>UAS-Atg1^I/+</i> ; <i>A58-Gal4</i> , <i>UAS-Src-GFP</i> , <i>UAS-DsRed2-Nuc/UAS-Atg1^{6B}</i>
8 A	<i>w</i> ¹¹¹⁸ ; <i>UAS-Atg1^I/+</i> ; <i>A58-Gal4</i> , <i>UAS-Src-GFP</i> , <i>UAS-DsRed2-Nuc/UAS-rictor^J</i>
8 A	<i>w</i> ¹¹¹⁸ ; <i>UAS-Atg5^I/+</i> ; <i>A58-Gal4</i> , <i>UAS-Src-GFP</i> , <i>UAS-DsRed2-Nuc/+</i>
8 A	<i>w</i> ¹¹¹⁸ ; <i>UAS-Atg5^I/+</i> ; <i>A58-Gal4</i> , <i>UAS-Src-GFP</i> , <i>UAS-DsRed2-Nuc/UAS-Tor^J</i>
8 A	<i>w</i> ¹¹¹⁸ ; <i>UAS-Atg5^I/+</i> ; <i>A58-Gal4</i> , <i>UAS-Src-GFP</i> , <i>UAS-DsRed2-Nuc/UAS-raptor^J</i>

Table 2 (continued)

Figure no. or Movie no.	Fly stock/cross
8 A	<i>w</i> ¹¹¹⁸ ; <i>UAS-Atg5^I/+</i> ; <i>A58-Gal4</i> , <i>UAS-Src-GFP</i> , <i>UAS-DsRed2-Nuc/UAS-Atg1^{6B}</i>
8 A	<i>w</i> ¹¹¹⁸ ; <i>UAS-Atg5^I/+</i> ; <i>A58-Gal4</i> , <i>UAS-Src-GFP</i> , <i>UAS-DsRed2-Nuc/ UAS-Atg1^{GS}</i> , <i>UAS-GFP</i>
8 A	<i>w</i> ¹¹¹⁸ ; <i>UAS-Atg5^I/+</i> ; <i>A58-Gal4</i> , <i>UAS-Src-GFP</i> , <i>UAS-DsRed2-Nuc/UAS-rictor^J</i>
8 B, C, D	<i>w</i> ¹¹¹⁸ ; <i>UAS-GFP/+</i> ; <i>A58-Gal4/+</i> (Control)
8 B, C, D	<i>w</i> ¹¹¹⁸ ; <i>UAS-Atg5^I/+</i> ; <i>A58-Gal4/UAS-Atg1^{GS}</i> , <i>UAS-GFP</i>
9 A	<i>w</i> ¹¹¹⁸ ; <i>endo:DE-cad-GFP</i> , <i>endo:Sqh-mCherry/UAS-Atg5^I</i> ; <i>A58-Gal4/+</i>
9 A	<i>w</i> ¹¹¹⁸ ; <i>endo:DE-cad-GFP</i> , <i>endo:Sqh-mCherry/UAS-Atg5^I</i> ; <i>A58-Gal4/ UAS-Tor^J</i>
9 A	<i>w</i> ¹¹¹⁸ ; <i>endo:DE-cad-GFP</i> , <i>endo:Sqh-mCherry/UAS-Atg5^I</i> ; <i>A58-Gal4/UAS-raptor^J</i>
9 A	<i>w</i> ¹¹¹⁸ ; <i>endo:DE-cad-GFP</i> , <i>endo:Sqh-mCherry/UAS-Atg5^I</i> ; <i>A58-Gal4/UAS-Atg1^{6B}</i>
9 A	<i>w</i> ¹¹¹⁸ ; <i>endo:DE-cad-GFP</i> , <i>endo:Sqh-mCherry/UAS-Atg5^I</i> ; <i>A58-Gal4/UAS-rictor^J</i>
9 B	<i>w</i> ¹¹¹⁸ ; +; <i>A58-Gal4</i> , <i>UAS-DsRed2-Nuc/+</i> (Control)
9 B	<i>w</i> ¹¹¹⁸ ; <i>UAS-Atg5^I/+</i> ; <i>A58-Gal4</i> , <i>UAS-DsRed2-Nuc/+</i>
9 B	<i>w</i> ¹¹¹⁸ ; <i>UAS-Atg5^I/+</i> ; <i>A58-Gal4</i> , <i>UAS-DsRed2-Nuc/UAS-Tor^J</i>
9 B	<i>w</i> ¹¹¹⁸ ; <i>UAS-Atg5^I/+</i> ; <i>A58-Gal4</i> , <i>UAS-DsRed2-Nuc/UAS-raptor^J</i>
9 B	<i>w</i> ¹¹¹⁸ ; <i>UAS-Atg5^I/+</i> ; <i>A58-Gal4</i> , <i>UAS-DsRed2-Nuc/UAS-Atg1^{6B}</i>
9 B	<i>w</i> ¹¹¹⁸ ; <i>UAS-Atg5^I/+</i> ; <i>A58-Gal4</i> , <i>UAS-DsRed2-Nuc/UAS-rictor^J</i>
9 C, D	<i>w</i> ¹¹¹⁸ ; +; <i>A58-Gal4</i> , <i>UAS-DsRed2-Nuc/+</i> (Control)
9 C, D	<i>w</i> ¹¹¹⁸ ; <i>UAS-TSC1</i> , <i>UAS-TSC2/+</i> ; <i>A58-Gal4</i> , <i>UAS-DsRed2-Nuc/+</i>
9 C, D	<i>w</i> ¹¹¹⁸ ; <i>UAS-Tor^{DN}/+</i> ; <i>A58-Gal4</i> , <i>UAS-DsRed2-Nuc/+</i>
9 C, D	<i>w</i> ¹¹¹⁸ ; +; <i>A58-Gal4</i> , <i>UAS-DsRed2-Nuc/UAS-Tor^J</i>
9 C, D	<i>w</i> ¹¹¹⁸ ; +; <i>A58-Gal4</i> , <i>UAS-DsRed2-Nuc/UAS-raptor^J</i>
9 C, D	<i>w</i> ¹¹¹⁸ ; +; <i>A58-Gal4</i> , <i>UAS-DsRed2-Nuc/UAS-Atg1^{6B}</i>
9 C, D	<i>w</i> ¹¹¹⁸ ; +; <i>A58-Gal4</i> , <i>UAS-DsRed2-Nuc/UAS-rictor^J</i>
9 C, D	<i>w</i> ¹¹¹⁸ ; <i>UAS-Atg1^I/+</i> ; <i>A58-Gal4</i> , <i>UAS-DsRed2-Nuc/UAS-Atg1^{6B}</i>
9 C, D	<i>w</i> ¹¹¹⁸ ; <i>UAS-Atg5^I/+</i> ; <i>A58-Gal4</i> , <i>UAS-DsRed2-Nuc/UAS-Atg1^{6B}</i>
10 A, B	<i>w</i> ¹¹¹⁸ ; <i>endo:FasIII-GFP/UAS-mCherry-Ag8a</i> ; <i>A58-Gal4/+</i> (Control)
10 C	<i>w</i> ¹¹¹⁸ ; +; <i>A58-Gal4</i> , <i>UAS-Src-GFP</i> , <i>UAS-DsRed2-Nuc/UAS-Atg1^{6B}</i>
S1	<i>w</i> ¹¹¹⁸ ; <i>UAS-mCherry-Ag8a/+</i> ; <i>A58-Gal4/+</i>
S2 A, B	<i>w</i> ¹¹¹⁸ ; <i>UAS-LAMP1-GFP/+</i> ; <i>A58-Gal4</i> , <i>UAS-DsRed2-Nuc/+</i> (Control)
S2 A, B	<i>w</i> ¹¹¹⁸ ; <i>UAS-LAMP1-GFP/UAS-TSC1</i> , <i>UAS-TSC2/+</i> ; <i>A58-Gal4</i> , <i>UAS-DsRed2-Nuc/+</i>
S2 A, B	<i>w</i> ¹¹¹⁸ ; <i>UAS-LAMP1-GFP/UAS-Tor^{DN}</i> ; <i>A58-Gal4</i> , <i>UAS-DsRed2-Nuc/+</i>

Table 2 (continued)

Figure no. or Movie no.	Fly stock/cross
S2 A, B	<i>w¹¹¹⁸</i> ; UAS-LAMP1-GFP/+; A58-Gal4, UAS-DsRed2-Nuc/UAS-Tor ^j
S2 A, B	<i>w¹¹¹⁸</i> ; UAS-LAMP1-GFP/+; A58-Gal4, UAS-DsRed2-Nuc/UAS-raptor ^j
S2 A, B	<i>w¹¹¹⁸</i> ; UAS-LAMP1-GFP/+; A58-Gal4, UAS-DsRed2-Nuc/UAS-Atg1 ^{6B}
S2 A, B	<i>w¹¹¹⁸</i> ; UAS-LAMP1-GFP/+; A58-Gal4, UAS-DsRed2-Nuc/UAS-rictor ^j
S2 C,	<i>w¹¹¹⁸</i> ; <i>tub:Gal80^{ts}/+</i> ; A58-Gal4, UAS-Src-GFP, UAS-DsRed2-Nuc/+ (Control)
S2 C,	<i>w¹¹¹⁸</i> ; <i>tub:Gal80^{ts}/+</i> ; A58-Gal4, UAS-Src-GFP, UAS-DsRed2-Nuc/UAS-Tor ^j
S2 C,	<i>w¹¹¹⁸</i> ; <i>tub:Gal80^{ts}/+</i> ; A58-Gal4, UAS-Src-GFP, UAS-DsRed2-Nuc/UAS-raptor ^j
S2 C,	<i>w¹¹¹⁸</i> ; <i>tub:Gal80^{ts}/+</i> ; A58-Gal4, UAS-Src-GFP, UAS-DsRed2-Nuc/UAS-Atg1 ^{6B}
S3 A, B	<i>w¹¹¹⁸</i> ; +; A58-Gal4, UAS-DsRed2-Nuc/+ (Control)
S3 A, B	<i>w¹¹¹⁸</i> ; UAS-Tor ^{DN} /+; A58-Gal4, UAS-DsRed2-Nuc/+
S3 C	<i>w¹¹¹⁸</i> ; +; A58-Gal4/+ (Control)
S3 C	<i>w¹¹¹⁸</i> ; +; A58-Gal4/ UAS-Atg1 ^{6B}
S3 D	<i>w¹¹¹⁸</i> ; <i>endo:Nrg-GFP</i> ; +; A58-Gal4/+ (Control)
S3 D	<i>w¹¹¹⁸</i> ; <i>endo:Nrg-GFP</i> ; +; A58-Gal4/UAS-Atg1 ^{6B}
S3 E	<i>w¹¹¹⁸</i> ; <i>endo:DE-cad-GFP</i> , <i>endo:Sqh-mCherry</i> /+; A58-Gal4/+ (Control)
S3 E	<i>w¹¹¹⁸</i> ; <i>endo:DE-cad-GFP</i> , <i>endo:Sqh-mCherry</i> /+; A58-Gal4/UAS-Tor ^j
S3 E	<i>w¹¹¹⁸</i> ; <i>endo:DE-cad-GFP</i> , <i>endo:Sqh-mCherry</i> /+; A58-Gal4/UAS-TSC1 ^l
S3 E	<i>w¹¹¹⁸</i> ; <i>endo:DE-cad-GFP</i> , <i>endo:Sqh-mCherry</i> /UAS-RhoA ^l ; A58-Gal4/+
S3 E	<i>w¹¹¹⁸</i> ; <i>endo:DE-cad-GFP</i> , <i>endo:Sqh-mCherry</i> /UAS-Rok ^l ; A58-Gal4/+
S3 E	<i>w¹¹¹⁸</i> ; <i>endo:DE-cad-GFP</i> , <i>endo:Sqh-mCherry</i> /+; A58-Gal4/UAS-S6K ^{CA}
S4 A	<i>w¹¹¹⁸</i> ; +; A58-Gal4, UAS-Src-GFP, UAS-DsRed2-Nuc/+ (Control)
S4 A	<i>w¹¹¹⁸</i> ; +; A58-Gal4, UAS-Src-GFP, UAS-DsRed2-Nuc/UAS-Atg1 ^{6B}
S4 B	<i>w¹¹¹⁸</i> ; +; A58-Gal4, UAS-mCD8-GFP/+ (Control)
S4 B	<i>w¹¹¹⁸</i> ; +; A58-Gal4, UAS-mCD8-GFP/UAS-Atg1 ^{6B}
S4 C	<i>w¹¹¹⁸</i> ; +; A58-Gal4, UAS-DsRed2-Nuc/+ (Control)
S4 C	<i>w¹¹¹⁸</i> ; +; A58-Gal4, UAS-DsRed2-Nuc/UAS-Tor ^j
S4 C	<i>w¹¹¹⁸</i> ; +; A58-Gal4, UAS-DsRed2-Nuc/UAS-raptor ^j
S4 C	<i>w¹¹¹⁸</i> ; +; A58-Gal4, UAS-DsRed2-Nuc/UAS-Atg1 ^{6B}
S4 C	<i>w¹¹¹⁸</i> ; +; A58-Gal4, UAS-DsRed2-Nuc/UAS-rictor ^j
S5 A	<i>w¹¹¹⁸</i> ; <i>endo:DE-cad-GFP</i> , <i>endo:Sqh-mCherry</i> /+; A58-Gal4/+ (Control)
S5 A	<i>w¹¹¹⁸</i> ; <i>endo:DE-cad-GFP</i> , <i>endo:Sqh-mCherry</i> /+; A58-Gal4/UAS-Tor ^j
S5 A	<i>w¹¹¹⁸</i> ; <i>endo:DE-cad-GFP</i> , <i>endo:Sqh-mCherry</i> /+; A58-Gal4/UAS-raptor ^j

Table 2 (continued)

Figure no. or Movie no.	Fly stock/cross
S5 A	<i>w¹¹¹⁸</i> ; <i>endo:DE-cad-GFP</i> , <i>endo:Sqh-mCherry</i> /+; A58-Gal4/UAS-Atg1 ^{6B} , UAS-GFP
S5 A	<i>w¹¹¹⁸</i> ; <i>endo:DE-cad-GFP</i> , <i>endo:Sqh-mCherry</i> /+; A58-Gal4/UAS-Atg1 ^{6B}
S5 B	<i>w¹¹¹⁸</i> ; +; A58-Gal4, UAS-Src-GFP, UAS-DsRed2-Nuc/+ (Control)
S5 B	<i>w¹¹¹⁸</i> ; +; A58-Gal4, UAS-Src-GFP, UAS-DsRed2-Nuc/UAS-Atg1 ^{6B}
S5 B	<i>w¹¹¹⁸</i> ; +; A58-Gal4, UAS-Src-GFP, UAS-DsRed2-Nuc/UAS-rictor ^j
S6 A, B	<i>w¹¹¹⁸</i> ; +; A58-Gal4, UAS-Src-GFP, UAS-DsRed2-Nuc/+ (Control)
S6 A, B	<i>w¹¹¹⁸</i> ; UAS-Tor ^{DN} /+; A58-Gal4, UAS-Src-GFP, UAS-DsRed2-Nuc/+
S6 A, B	<i>w¹¹¹⁸</i> ; +; A58-Gal4, UAS-Src-GFP, UAS-DsRed2-Nuc/UAS-raptor ^j
S6 A, B	<i>w¹¹¹⁸</i> ; +; A58-Gal4, UAS-Src-GFP, UAS-DsRed2-Nuc/UAS-Atg1 ^{6B} , UAS-GFP
S6 A, B	<i>w¹¹¹⁸</i> ; +; A58-Gal4, UAS-Src-GFP, UAS-DsRed2-Nuc/UAS-Atg1 ^{6B}
S6 C	<i>w¹¹¹⁸</i> ; UAS-GFP/+; A58-Gal4/+ (Control)
S6 C	<i>w¹¹¹⁸</i> ; +; A58-Gal4/UAS-Atg1 ^{6B} , UAS-GFP
S6 D, E	<i>w¹¹¹⁸</i> ; NP1-Gal4/UAS-GFP-Baz; + (Control)
S6 D, E	<i>w¹¹¹⁸</i> ; NP1-Gal4/UAS-GFP-Baz; +/UAS-raptor ^j
S6 D, E	<i>w¹¹¹⁸</i> ; NP1-Gal4/UAS-GFP-Baz; UAS-Atg1 ^{6B} /+
S6 E	<i>w¹¹¹⁸</i> ; NP1-Gal4/UAS-TSC1, UAS-TSC2; UAS-GFP-Baz/+
S7 A	<i>w¹¹¹⁸</i> ; UAS-mito-GFP/+; A58-Gal4, UAS-DsRed2-Nuc/+ (Control)
S7 A	<i>w¹¹¹⁸</i> ; UAS-mito-GFP/UAS-Tor ^{DN} ; A58-Gal4, UAS-DsRed2-Nuc/+
S7 A	<i>w¹¹¹⁸</i> ; UAS-mito-GFP/+; A58-Gal4, UAS-DsRed2-Nuc/UAS-raptor ^j
S7 A	<i>w¹¹¹⁸</i> ; UAS-mito-GFP/+; A58-Gal4, UAS-DsRed2-Nuc/UAS-Atg1 ^{6B}
S7 B, C	<i>w¹¹¹⁸</i> ; UAS-RFP-KDEL/+; A58-Gal4/+ (Control)
S7 B, C	<i>w¹¹¹⁸</i> ; UAS-RFP-KDEL/UAS-TSC1, UAS-TSC2; A58-Gal4/+
S7 B, C	<i>w¹¹¹⁸</i> ; UAS-RFP-KDEL/UAS-Tor ^{DN} ; A58-Gal4/+
S7 B, C	<i>w¹¹¹⁸</i> ; UAS-RFP-KDEL/+; A58-Gal4/UAS-Tor ^j
S7 B, C	<i>w¹¹¹⁸</i> ; UAS-RFP-KDEL/+; A58-Gal4/UAS-raptor ^j
S7 B, C	<i>w¹¹¹⁸</i> ; UAS-RFP-KDEL/+; A58-Gal4/UAS-Atg1 ^{6B}
S7 B, C	<i>w¹¹¹⁸</i> ; UAS-RFP-KDEL/+; A58-Gal4/UAS-rictor ^j
S7 D, E	<i>w¹¹¹⁸</i> ; UAS-GFP-Golgi/+; A58-Gal4/+ (Control)
S7 D, E	<i>w¹¹¹⁸</i> ; UAS-GFP-Golgi/UAS-TSC1, UAS-TSC2; A58-Gal4/+
S7 D, E	<i>w¹¹¹⁸</i> ; UAS-GFP-Golgi/UAS-Tor ^{DN} ; A58-Gal4/+
S7 D, E	<i>w¹¹¹⁸</i> ; UAS-GFP-Golgi/+; A58-Gal4/UAS-Tor ^j
S7 D, E	<i>w¹¹¹⁸</i> ; UAS-GFP-Golgi/+; A58-Gal4/UAS-raptor ^j
S7 D, E	<i>w¹¹¹⁸</i> ; UAS-GFP-Golgi/+; A58-Gal4/UAS-Atg1 ^{6B}
S8 A	<i>w¹¹¹⁸</i> ; <i>endo:Klaroid-GFP</i> /+; A58-Gal4, UAS-DsRed2-Nuc/+ (Control)

Table 2 (continued)

Figure no. or Movie no.	Fly stock/cross
S8 A	$w^{1118}; \text{endo:Klaroid-GFP/+}; A58-Gal4, UAS-DsRed2-Nuc/UAS-Atg1^{6B}$
S8 B, C	$w^{1118}; +; A58-Gal4, UAS-Src-GFP, UAS-DsRed2-Nuc/+$ (Control)
S8 B, C	$w^{1118}; +; A58-Gal4, UAS-Src-GFP, UAS-DsRed2-Nuc/UAS-raptor^j$
S8 B, C	$w^{1118}; +; A58-Gal4, UAS-Src-GFP, UAS-DsRed2-Nuc/UAS-Atg1^{GS}, UAS-GFP$
S8 B, C	$w^{1118}; +; A58-Gal4, UAS-Src-GFP, UAS-DsRed2-Nuc/UAS-Atg1^{6B}$
S8 D	$w^{1118}; \text{endo:His2Au-RFP/+}; A58-Gal4/+$
S8 D	$w^{1118}; \text{endo:His2Au-RFP/ UAS-Tor}^{DN}; A58-Gal4/+$ (Control)
S8 D	$w^{1118}; \text{endo:His2Au-RFP/+}; A58-Gal4/UAS-Atg1^{GS}, UAS-GFP$
S8 D	$w^{1118}; \text{endo:His2Au-RFP/+}; A58-Gal4/ UAS-Atg1^{6B}$
S8 D	$w^{1118}; \text{endo:His2Au-RFP/+}; A58-Gal4/UAS-rictor^j$
S8 E	$w^{1118}; UAS-RFP-LamB/+; A58-Gal4/+$ (Control)
S8 E	$w^{1118}; UAS-RFP-LamB/+; A58-Gal4/UAS-Atg1^{6B}$
S8 E	$w^{1118}; UAS-RFP-LamB/+; A58-Gal4/ UAS-Atg1^{GS}, UAS-GFP$
S9 A	$w^{1118}; +; A58-Gal4, UAS-Src-GFP, UAS-DsRed2-Nuc/+$ (Control)
S9 A	$w^{1118}; UAS-Tor^{DN}/+; A58-Gal4, UAS-Src-GFP, UAS-DsRed2-Nuc/+$
S9 A	$w^{1118}; UAS-raptor^{j-2}/+; A58-Gal4, UAS-Src-GFP, UAS-DsRed2-Nuc/+$
S9 A	$w^{1118}; +; A58-Gal4, UAS-Src-GFP, UAS-DsRed2-Nuc/UAS-S6K^{CA}$
S9 A	$w^{1118}; UAS-Tor^{DN}/+; A58-Gal4, UAS-Src-GFP, UAS-DsRed2-Nuc/UAS-S6K^{CA}$
S9 A	$w^{1118}; UAS-raptor^{j-2}/+; A58-Gal4, UAS-Src-GFP, UAS-DsRed2-Nuc/UAS-S6K^{CA}$
S9 A	$w^{1118}; +; A58-Gal4, UAS-Src-GFP, UAS-DsRed2-Nuc/UAS-rictor^j$
S9 A	$w^{1118}; UAS-Tor^{DN}/+; A58-Gal4, UAS-Src-GFP, UAS-DsRed2-Nuc/UAS-rictor^j$
S9 A	$w^{1118}; UAS-raptor^{j-2}/+; A58-Gal4, UAS-Src-GFP, UAS-DsRed2-Nuc/UAS-rictor^j$
S9 A	$w^{1118}; +; A58-Gal4, UAS-Src-GFP, UAS-DsRed2-Nuc/UAS-Atg12^j$
S9 A	$w^{1118}; UAS-Tor^{DN}/+; A58-Gal4, UAS-Src-GFP, UAS-DsRed2-Nuc/UAS-Atg12^j$
S9 A	$w^{1118}; UAS-raptor^{j-2}/+; A58-Gal4, UAS-Src-GFP, UAS-DsRed2-Nuc/UAS-Atg12^j$
S9 A	$w^{1118}; +; A58-Gal4, UAS-Src-GFP, UAS-DsRed2-Nuc/UAS-Atg7^i$
S9 A	$w^{1118}; UAS-Tor^{DN}/+; A58-Gal4, UAS-Src-GFP, UAS-DsRed2-Nuc/UAS-Atg7^i$
S9 A	$w^{1118}; UAS-raptor^{j-2}/+; A58-Gal4, UAS-Src-GFP, UAS-DsRed2-Nuc/UAS-Atg7^i$
S9 A	$w^{1118}; UAS-Atg1^i/+; A58-Gal4, UAS-Src-GFP, UAS-DsRed2-Nuc/UAS-Atg7^i$

Table 2 (continued)

Figure no. or Movie no.	Fly stock/cross
S9 A	$w^{1118}; UAS-Atg6^i/+; A58-Gal4, UAS-Src-GFP, UAS-DsRed2-Nuc/+$
S9 A	$w^{1118}; UAS-Atg6^i/+; A58-Gal4, UAS-Src-GFP, UAS-DsRed2-Nuc/UAS-Tor^i$
S9 A	$w^{1118}; UAS-Atg6^i/+; A58-Gal4, UAS-Src-GFP, UAS-DsRed2-Nuc/UAS-raptor^i$
S9 A	$w^{1118}; UAS-Atg6^i/+; A58-Gal4, UAS-Src-GFP, UAS-DsRed2-Nuc/UAS-Atg1^{6B}$
S9 B, C	$w^{1118}; UAS-GFP-Atg8a/+; A58-Gal4/+$ (Control)
S9 B	$w^{1118}; UAS-GFP-Atg8a/+; A58-Gal4/UAS-Tor^i$
S9 B	$w^{1118}; UAS-GFP-Atg8a/+; A58-Gal4/UAS-raptor^i$
S9 B	$w^{1118}; UAS-GFP-Atg8a/+; A58-Gal4/UAS-Atg1^{6B}$
S9 B, C	$w^{1118}; UAS-GFP-Atg8a/UAS-Atg1^i; A58-Gal4/+$
S9 B, C	$w^{1118}; UAS-GFP-Atg8a/UAS-Atg1^i; A58-Gal4/UAS-Tor^i$
S9 B, C	$w^{1118}; UAS-GFP-Atg8a/UAS-Atg1^i; A58-Gal4/UAS-raptor^i$
S9 B, C	$w^{1118}; UAS-GFP-Atg8a/UAS-Atg1^i; A58-Gal4/UAS-Atg1^{6B}$
S9 B, C	$w^{1118}; UAS-GFP-Atg8a/UAS-Atg5^i; A58-Gal4/+$
S9 B, C	$w^{1118}; UAS-GFP-Atg8a/UAS-Atg5^i; A58-Gal4/UAS-Tor^i$
S9 B, C	$w^{1118}; UAS-GFP-Atg8a/UAS-Atg5^i; A58-Gal4/UAS-raptor^i$
S9 B, C	$w^{1118}; UAS-GFP-Atg8a/UAS-Atg5^i; A58-Gal4/UAS-Atg1^{6B}$
S9 B, C	$w^{1118}; UAS-GFP-Atg8a/UAS-Atg6^i; A58-Gal4/+$
S9 B, C	$w^{1118}; UAS-GFP-Atg8a/UAS-Atg6^i; A58-Gal4/UAS-Tor^i$
S9 B, C	$w^{1118}; UAS-GFP-Atg8a/UAS-Atg6^i; A58-Gal4/UAS-raptor^i$
S9 B, C	$w^{1118}; UAS-GFP-Atg8a/UAS-Atg6^i; A58-Gal4/UAS-Atg1^{6B}$
S9 B	$w^{1118}; UAS-GFP-Atg8a/UAS-Tor^{DN}; A58-Gal4/+$
S9 B, C	$w^{1118}; UAS-GFP-Atg8a/+; A58-Gal4/UAS-Atg7^i$
S9 B, C	$w^{1118}; UAS-GFP-Atg8a/UAS-Tor^{DN}; A58-Gal4/UAS-Atg7^i$
S9 B, C	$w^{1118}; UAS-GFP-Atg8a/UAS-raptor^{j-2}; A58-Gal4/UAS-Atg7^i$
S10 A	$w^{1118}; +; A58-Gal4, UAS-Src-GFP, UAS-DsRed2-Nuc/+$ (Control)
S10 A	$w^{1118}; +; A58-Gal4, UAS-Src-GFP, UAS-DsRed2-Nuc/UAS-Tor^i$
S10 A	$w^{1118}; +; A58-Gal4, UAS-Src-GFP, UAS-DsRed2-Nuc/UAS-raptor^i$
S10 A	$w^{1118}; +; A58-Gal4, UAS-Src-GFP, UAS-DsRed2-Nuc/UAS-Atg1^{6B}$
S10 A	$w^{1118}; +; A58-Gal4, UAS-Src-GFP, UAS-DsRed2-Nuc/UAS-rictor^j$
S10 A	$w^{1118}; UAS-Atg1^i/+; A58-Gal4, UAS-Src-GFP, UAS-DsRed2-Nuc/+$
S10 A	$w^{1118}; UAS-Atg1^i/+; A58-Gal4, UAS-Src-GFP, UAS-DsRed2-Nuc/UAS-Tor^i$
S10 A	$w^{1118}; UAS-Atg1^i/+; A58-Gal4, UAS-Src-GFP, UAS-DsRed2-Nuc/UAS-raptor^i$
S10 A	$w^{1118}; UAS-Atg1^i/+; A58-Gal4, UAS-Src-GFP, UAS-DsRed2-Nuc/UAS-Atg1^{6B}$
S10 A	$w^{1118}; UAS-Atg1^i/+; A58-Gal4, UAS-Src-GFP, UAS-DsRed2-Nuc/UAS-rictor^j$

Table 2 (continued)

Figure no. or Movie no.	Fly stock/cross
S10 A	$w^{1118}; UAS-Atg5^j/+; A58-Gal4, UAS-Src-GFP, UAS-DsRed2-Nuc/+$
S10 A	$w^{1118}; UAS-Atg5^j/+; A58-Gal4, UAS-Src-GFP, UAS-DsRed2-Nuc/UAS-Tor^j$
S10 A	$w^{1118}; UAS-Atg5^j/+; A58-Gal4, UAS-Src-GFP, UAS-DsRed2-Nuc/UAS-raptor^j$
S10 A	$w^{1118}; UAS-Atg5^j/+; A58-Gal4, UAS-Src-GFP, UAS-DsRed2-Nuc/UAS-Atg1^{6B}$
S10 A	$w^{1118}; UAS-Atg5^j/+; A58-Gal4, UAS-Src-GFP, UAS-DsRed2-Nuc/UAS-ric1^j$
S10 B	$w^{1118}; endo:DE-cad-GFP, endo:Sqh-mCherry/UAS-Atg1^j; A58-Gal4/+$
S10 B	$w^{1118}; endo:DE-cad-GFP, endo:Sqh-mCherry/UAS-Atg1^j; A58-Gal4/ UAS-Tor^j$
S10 B	$w^{1118}; endo:DE-cad-GFP, endo:Sqh-mCherry/UAS-Atg1^j; A58-Gal4/UAS-raptor^j$
S10 B	$w^{1118}; endo:DE-cad-GFP, endo:Sqh-mCherry/UAS-Atg1^j; A58-Gal4/UAS-Atg1^{6B}$
S10 B	$w^{1118}; endo:DE-cad-GFP, endo:Sqh-mCherry/UAS-Atg1^j; A58-Gal4/UAS-ric1^j$
S11	$w^{1118}; +; A58-Gal4, UAS-Src-GFP, UAS-DsRed2-Nuc/+$ (Control)
S11	$w^{1118}; UAS-Rheb^{AV4}/+; A58-Gal4, UAS-Src-GFP, UAS-DsRed2-Nuc/+$
S11	$w^{1118}; UAS-TSC1^{i-2}/+; A58-Gal4, UAS-Src-GFP, UAS-DsRed2-Nuc/+$
S11	$w^{1118}; +; A58-Gal4, UAS-Src-GFP, UAS-DsRed2-Nuc/ UAS-TSC1^i$
S11	$w^{1118}; +; A58-Gal4, UAS-Src-GFP, UAS-DsRed2-Nuc/UAS-Atg1^{6B}$
S11	$w^{1118}; UAS-Rheb^{AV4}/+; A58-Gal4, UAS-Src-GFP, UAS-DsRed2-Nuc/UAS-Atg1^{6B}$
S11	$w^{1118}; UAS-TSC1^{i-2}/+; A58-Gal4, UAS-Src-GFP, UAS-DsRed2-Nuc/UAS-Atg1^{6B}$
S12 A, B	$w^{1118}; UAS-GFP-Atg8a/+; A58-Gal4/+$ (Control)
S12 A, B	$w^{1118}; UAS-GFP-Atg8a/UAS-Tor^{DN}; A58-Gal4/+$
S12 A, B	$w^{1118}; UAS-GFP-Atg8a/+; A58-Gal4/UAS-Tor^j$
S12 A, B	$w^{1118}; UAS-GFP-Atg8a/+; A58-Gal4/UAS-raptor^j$
S12 A, B	$w^{1118}; UAS-GFP-Atg8a/+; A58-Gal4/UAS-Atg1^{6B}$
S12 A, B	$w^{1118}; UAS-GFP-Atg8a/+; A58-Gal4/UAS-ric1^j$
S12 C	$w^{1118}; +; A58-Gal4, UAS-Src-GFP, UAS-DsRed2-Nuc/+$ (Control)
S12 C	$w^{1118}; UAS-TSC1, UAS-TSC2/+; A58-Gal4, UAS-Src-GFP, UAS-DsRed2-Nuc/+$
S12 C	$w^{1118}; +; A58-Gal4, UAS-Src-GFP, UAS-DsRed2-Nuc/UAS-Tor^j$
S12 C	$w^{1118}; +; A58-Gal4, UAS-Src-GFP, UAS-DsRed2-Nuc/UAS-raptor^j$
S12 C	$w^{1118}; +; A58-Gal4, UAS-Src-GFP, UAS-DsRed2-Nuc/UAS-Atg1^{6B}$
S12 D	$w^{1118}; +; A58-Gal4, UAS-Src-GFP, UAS-DsRed2-Nuc/+$ (Control)

Table 2 (continued)

Figure no. or Movie no.	Fly stock/cross
S12 D	$w^{1118}; UAS-Syx17^j/+; A58-Gal4, UAS-Src-GFP, UAS-DsRed2-Nuc/+$
S12 D	$w^{1118}; UAS-Vamp7^j/+; A58-Gal4, UAS-Src-GFP, UAS-DsRed2-Nuc/+$
S12 D	$w^{1118}; UAS-Snap29^j/+; A58-Gal4, UAS-Src-GFP, UAS-DsRed2-Nuc/+$
S12 D	$w^{1118}; UAS-Snap29^{i-2}/+; A58-Gal4, UAS-Src-GFP, UAS-DsRed2-Nuc/+$
S12 D	$w^{1118}; +; A58-Gal4, UAS-Src-GFP, UAS-DsRed2-Nuc/UAS-Atg1^{6B}$
S12 D	$w^{1118}; UAS-Syx17^j/+; A58-Gal4, UAS-Src-GFP, UAS-DsRed2-Nuc/UAS-Atg1^{6B}$
S12 D	$w^{1118}; UAS-Vamp7^j/+; A58-Gal4, UAS-Src-GFP, UAS-DsRed2-Nuc/UAS-Atg1^{6B}$
S12 D	$w^{1118}; UAS-Snap29^j/+; A58-Gal4, UAS-Src-GFP, UAS-DsRed2-Nuc/UAS-Atg1^{6B}$
S12 D	$w^{1118}; UAS-Snap29^{i-2}/+; A58-Gal4, UAS-Src-GFP, UAS-DsRed2-Nuc/UAS-Atg1^{6B}$
S13 A	$w^{1118}; endo:FasIII-GFP/UAS-mCherry-Ag8a; A58-Gal4/+$
S13 B, C	$w^{1118}; UAS-mCherry-Ag8a/+; A58-Gal4, UAS-mCSD8-GFP/+$
S14 A	$w^{1118}; endo:DE-cad-GFP, endo:Sqh-mCherry/+; A58-Gal4/UAS-Atg1^{GS}, UAS-GFP$
S14 A	$w^{1118}; endo:DE-cad-GFP, endo:Sqh-mCherry/UAS-Sqa^{KA}; A58-Gal4/UAS-Atg1^{GS}, UAS-GFP$
S14 B	$w^{1118}; UAS-Sqa^{KA}/+; A58-Gal4, UAS-Src-GFP, UAS-DsRed2-Nuc/+$
S14 B	$w^{1118}; UAS-Sqa^{KA}/+; A58-Gal4, UAS-Src-GFP, UAS-DsRed2-Nuc/UAS-Tor^j$
S14 B	$w^{1118}; UAS-Sqa^{KA}/+; A58-Gal4, UAS-Src-GFP, UAS-DsRed2-Nuc/UAS-raptor^j$
S14 B	$w^{1118}; UAS-Sqa^{KA}/+; A58-Gal4, UAS-Src-GFP, UAS-DsRed2-Nuc/UAS-Atg1^{6B}$
S14 B	$w^{1118}; UAS-Rok^j/+; A58-Gal4, UAS-Src-GFP, UAS-DsRed2-Nuc/+$
S14 B	$w^{1118}; UAS-Rok^j/+; A58-Gal4, UAS-Src-GFP, UAS-DsRed2-Nuc/UAS-Tor^j$
S14 B	$w^{1118}; UAS-Rok^j/+; A58-Gal4, UAS-Src-GFP, UAS-DsRed2-Nuc/UAS-raptor^j$
S14 B	$w^{1118}; UAS-Rok^j/+; A58-Gal4, UAS-Src-GFP, UAS-DsRed2-Nuc/UAS-Atg1^{6B}$
S15 A	$w^{1118}; endo:DE-cad-GFP, endo:Sqh-mCherry/UAS-Atg1^j; A58-Gal4/+$
S15 A	$w^{1118}; endo:DE-cad-GFP, endo:Sqh-mCherry/UAS-Atg1^j; A58-Gal4/ UAS-Tor^j$
S15 A	$w^{1118}; endo:DE-cad-GFP, endo:Sqh-mCherry/UAS-Atg1^j; A58-Gal4/UAS-raptor^j$
S15 A	$w^{1118}; endo:DE-cad-GFP, endo:Sqh-mCherry/UAS-Atg1^j; A58-Gal4/UAS-Atg1^{6B}$
S15 B	$w^{1118}; endo:DE-cad-GFP, endo:Sqh-mCherry/UAS-Atg5^j; A58-Gal4/+$
S15 B	$w^{1118}; endo:DE-cad-GFP, endo:Sqh-mCherry/UAS-Atg5^j; A58-Gal4/ UAS-Tor^j$

Table 2 (continued)

Figure no. or Movie no.	Fly stock/cross
S15 B	$w^{1118}; endo:DE-cad-GFP, endo:Sqh-mCherry/UAS-Atg5^1; A58-Gal4/UAS-raptor^f$
S15 B	$w^{1118}; endo:DE-cad-GFP, endo:Sqh-mCherry/UAS-Atg5^1; A58-Gal4/UAS-Atg1^{6B}$
Movie EV1	$w^{1118}; UAS-GFP-Atg8a/+; A58-Gal4/+$ (Control)
Movie EV1	$w^{1118}; UAS-GFP-Atg8a/UAS-Atg1^1; A58-Gal4/+$
Movie EV1	$w^{1118}; UAS-GFP-Atg8a/UAS-Atg5^1; A58-Gal4/+$
Movie EV1	$w^{1118}; UAS-GFP-Atg8a/UAS-Atg6^1; A58-Gal4/+$
Movie EV2	$w^{1118}; UAS-mCherry-Ag8a/+; A58-Gal4/+$
Movie EV3	$w^{1118}; +; A58-Gal4, UAS-Src-GFP, UAS-DsRed2-Nuc/+$ (Control)
Movie EV3	$w^{1118}; UAS-Atg1^1/+; A58-Gal4, UAS-Src-GFP, UAS-DsRed2-Nuc/+$
Movie EV3	$w^{1118}; UAS-Atg5^1/+; A58-Gal4, UAS-Src-GFP, UAS-DsRed2-Nuc/+$
Movie EV3	$w^{1118}; UAS-Atg6^1/+; A58-Gal4, UAS-Src-GFP, UAS-DsRed2-Nuc/+$
Movie EV4	$w^{1118}; endo:DE-Cad-GFP, endo:Sqh-mCherry/+; A58-Gal4/+$ (Control)
Movie EV4	$w^{1118}; endo:DE-Cad-GFP, endo:Sqh-mCherry/UAS-Atg1^1; A58-Gal4/+$
Movie EV4	$w^{1118}; endo:DE-Cad-GFP, endo:Sqh-mCherry/UAS-Atg5^1; A58-Gal4/+$
Movie EV5, EV6	$w^{1118}; hsf1p/+; act5c > y^+ > Gal4, UAS-GFP/+; ubi:DE-cad-RFP/+$ (Control)
Movie EV7	$w^{1118}; hsf1p/+; act5c > y^+ > Gal4, UAS-GFP/UAS-Atg1^1; ubi:DE-cad-RFP/+$
Movie EV8	$w^{1118}; hsf1p/+; act5c > y^+ > Gal4, UAS-GFP/UAS-Atg5^1; ubi:DE-cad-RFP/+$
Movie EV9	$w^{1118}; tub:Gal80^{5S}/+; A58-Gal4, UAS-Src-GFP, UAS-DsRed2-Nuc/UAS-Atg1^{6B}$
Movie EV10	$w^{1118}; endo:DE-cad-GFP, endo:Sqh-mCherry/+; A58-Gal4/+$ (Control)
Movie EV10	$w^{1118}; endo:DE-cad-GFP, endo:Sqh-mCherry/+; A58-Gal4/UAS-Atg1^{6S}, UAS-GFP$
Movie EV11	$w^{1118}; endo:DE-cad-GFP, endo:Sqh-mCherry/+; A58-Gal4/UAS-Tor^1$
Movie EV11	$w^{1118}; endo:DE-cad-GFP, endo:Sqh-mCherry/+; A58-Gal4/UAS-Atg1^{6B}$
Movie EV12	$w^{1118}; +; A58-Gal4, UAS-Src-GFP, UAS-DsRed2-Nuc/+$ (Control)
Movie EV12	$w^{1118}; +; A58-Gal4, UAS-Src-GFP, UAS-DsRed2-Nuc/UAS-Atg1^{6B}$
Movie EV13, EV14	$w^{1118}; UAS-GFP/+; A58-Gal4/+$ (Control)
Movie EV13, EV14, EV15	$w^{1118}; +; A58-Gal4/UAS-Atg1^{6S}, UAS-GFP$
Movie EV16	$w^{1118}; +; A58-Gal4, UAS-DsRed2-Nuc/UAS-Atg1^{6B}$
Movie EV17	$w^{1118}; UAS-Atg5^1/+; A58-Gal4/UAS-Atg1^{6S}, UAS-GFP$
Movie EV18, EV19	$w^{1118}; endo:FasIII-GFP/UAS-mCherry-Ag8a; A58-Gal4/+$
Movie EV20	$w^{1118}; UAS-mCherry-Ag8a/+; A58-Gal4, UAS-mCDB-GFP/+$

Table 2 (continued)

Figure no. or Movie no.	Fly stock/cross
Movie EV21	$w^{1118}; endo:DE-cad-GFP, endo:Sqh-mCherry/UAS-Atg1^1; A58-Gal4/+$
Movie EV21	$w^{1118}; endo:DE-cad-GFP, endo:Sqh-mCherry/UAS-Atg1^1; A58-Gal4/UAS-raptor^f$
Movie EV21	$w^{1118}; endo:DE-cad-GFP, endo:Sqh-mCherry/UAS-Atg1^1; A58-Gal4/UAS-Atg1^{6B}$
Movie EV22	$w^{1118}; endo:DE-cad-GFP, endo:Sqh-mCherry/UAS-Atg5^1; A58-Gal4/+$
Movie EV22	$w^{1118}; endo:DE-cad-GFP, endo:Sqh-mCherry/UAS-Atg5^1; A58-Gal4/ UAS-Tor^1$
Movie EV22	$w^{1118}; endo:DE-cad-GFP, endo:Sqh-mCherry/UAS-Atg5^1; A58-Gal4/UAS-Atg1^{6B}$

Image analysis

To quantify vesicles or puncta, the images were cropped to a uniform size and converted to 8-bit TIF files. Ilastik pixel-classifiers were trained separately using 6–15 images covering all genotypes for all markers. Separate classifiers were necessary since the nature of different “spots” is different. The *Batch Processing* function in Ilastik was used to process all the images and *Simple Segmentation* results were exported. Custom Python script was then used to identify the “spots” and to measure the number of spots in an area of 10,000 μm^2 . The codes are available at https://github.com/sourabh-bhide/Analyze_Vesicles.

In the FLIP experiment, image intensities were measured in the bleached area and the sum of intensities in the area plotted over the time. All measurements were normalized to the pre-bleached value in the ROI.

Data analysis

The plots were generated using the Python 3.7 library *Seaborn* (<https://seaborn.pydata.org/generated/seaborn.boxplot.html>). For statistical hypothesis testing, independent and non-parametric (Kruskal–Wallis) *t*-tests were performed for the mean number of spots in control and experimental conditions in the graphs in Figs 1D, 3C and 9D, Appendix Figs S2B and S9C. We assumed unequal sample size and unequal variances and calculations were performed using the Scipy library from Python 3.7 and GraphPad Prism version 8.1. For all other graphs (Appendix Figs S7D and G, and S12B) ordinary one-way ANOVA statistical tests were performed after we confirmed normality using the Shapiro–Wilk test ($\alpha = 0.05$). Values in this paper are presented as box plots. Box plot elements are: centre line, median; box limits, upper and lower quartiles; whiskers, 1.5 \times interquartile range; points, outliers. *P*-values are indicated as follows: **P* < 0.04; ***P* < 0.003; ****P* < 0.0002; *****P* < 0.0001 and lack of an asterisk or ns means non-significant (*P* > 0.123).

Transmission electron microscopy

For transmission electron microscopy, early L3 *Drosophila* larvae were fixed and cryo-immobilized by high-pressure freezing as previously described (Moussian & Schwarz, 2010).

Data availability

This study includes no data deposited in external repositories.

Expanded View for this article is available online.

Acknowledgements

We are grateful to A.J. Garcia-Saéz, F. Papagiannouli, M. Rembold, M. Graef, N.L. Kononenko, S. Eming, P. Ronchi, Y. Schwab and S. Roth for critical reading of the manuscript, comments and helpful discussions. We thank A. Wodarz, M.J. Galko, L. Partridge, M. Uhlirva, I. Bjedov, J. Großhans, G. Juhász, M. Peschmann and U. Thomas for antibodies, reagents and fly lines. We thank M. Kakanj for her photographic and graphical support, A. Schauss, F. Babatz, P. Zentis and C. Jüngst from the CECAD imaging facility in Cologne (University of Cologne, Cluster of Excellence in Ageing Research) for technical support and the Bloomington, VDRC and DGGR stock centres for fly strains. This work was funded by CMMC (Projekt-Nr. 16-RP, Fond 2635/8025/01) and CECAD through a grant by the Deutsche Forschungsgemeinschaft (DFG, German Research Foundation) under Germany's Excellence Strategy – EXC 2030 – 390661388, Gefördert durch die Deutsche Forschungsgemeinschaft (DFG) im Rahmen der Exzellenzstrategie des Bundes und der Länder - EXC 2030 – 390661388 to M.L. Open Access funding enabled and organized by Projekt DEAL.

Author contributions

Parisa Kakanj: Conceptualization; Data curation; Formal analysis; Validation; Investigation; Visualization; Methodology; Writing—original draft; Writing—review & editing. **Sourabh Bhide:** Software; Formal analysis. **Bernard Mousian:** Formal analysis; Methodology. **Maria Leptin:** Supervision; Funding acquisition; Writing—review & editing.

In addition to the CRediT author contributions listed above, the contributions in detail are:

PK conceived the project, designed the experiments, performed all experiments, and prepared the figures and tables. PK and BM performed TEM analysis and SB performed all image quantifications. PK and ML analysed and discussed the data and drafted the manuscript.

Disclosure and competing interests statement

The authors declare that they have no conflict of interest. Maria Leptin is the former director of EMBO and a co-founder of Review Commons. *The EMBO Journal* is editorially independent of EMBO.

References

- Allen EA, Baehrecke EH (2020) Autophagy in animal development. *Cell Death Differ* 27: 903–918
- Arsham AM, Neufeld TP (2009) A genetic screen in *Drosophila* reveals novel cytoprotective functions of the autophagy-lysosome pathway. *PLoS One* 4: e6068
- Bachmann A, Timmer M, Sierralta J, Pietrini G, Gundelfinger ED, Knust E, Thomas U (2004) Cell type-specific recruitment of *Drosophila* Lin-7 to distinct MAGUK-based protein complexes defines novel roles for Sdt and Dlg-S97. *J Cell Sci* 117: 1899–1909
- Barcelo H, Stewart MJ (2002) Altering *Drosophila* S6 kinase activity is consistent with a role for S6 kinase in growth. *Genesis* 34: 83–85
- Bejarano E, Yuste A, Patel B, Stout Jr RF, Spray DC, Cuervo AM (2014) Connexins modulate autophagosome biogenesis. *Nat Cell Biol* 16: 401–414
- Benton R, St Johnston D (2003) A conserved oligomerization domain in *Drosophila* Bazooka/PAR-3 is important for apical localization and epithelial polarity. *Curr Biol* 13: 1330–1334
- Besen-McNally R, Gjelsvik KJ, Losick VP (2021) Wound-induced polyploidization is dependent on Integrin-Yki signaling. *Biol Open* 10: bio055996
- Bjedov I, Cochemé HM, Foley A, Wieser D, Woodling NS, Castillo-Quan JI, Norvaisas P, Lujan C, Regan JC, Toivonen JM et al (2020) Fine-tuning autophagy maximises lifespan and is associated with changes in mitochondrial gene expression in *Drosophila*. *PLoS Genet* 16: e1009083
- Brandt A, Krohne G, Grosshans J (2008) The farnesylated nuclear proteins KUGELKERN and LAMIN B promote aging-like phenotypes in *Drosophila* flies. *Aging Cell* 7: 541–551
- Brandt A, Papagiannouli F, Wagner N, Wilsch-Bräuninger M, Braun M, Furlong EE, Loserth S, Wenzl C, Pilot F, Vogt N et al (2006) Developmental control of nuclear size and shape by Kugelkern and Kurzkern. *Curr Biol* 16: 543–552
- Buszczak M, Paterno S, Lighthouse D, Bachman J, Planck J, Owen S, Skora AD, Nystul TG, Ohlstein B, Allen A et al (2007) The carnegie protein trap library: a versatile tool for *Drosophila* developmental studies. *Genetics* 175: 1505–1531
- Cao B, Macones C, Mysorekar IU (2016) ATG16L1 governs placental infection risk and preterm birth in mice and women. *JCI Insight* 1: e86654
- Chang TK, Shrivage BV, Hayes SD, Powers CM, Simin RT, Wade Harper J, Baehrecke EH (2013) Uba1 functions in Atg7- and Atg3-independent autophagy. *Nat Cell Biol* 15: 1067–1078
- Chavez MN, Morales RA, Lopez-Crisosto C, Roa JC, Allende ML, Lavandero S (2020) Autophagy activation in zebrafish heart regeneration. *Sci Rep* 10: 2191
- Cole NB, Smith CL, Sciaky N, Terasaki M, Edidin M, Lippincott-Schwartz J (1996) Diffusional mobility of Golgi proteins in membranes of living cells. *Science* 273: 797–801
- Cox RT, Spradling AC (2003) A Balbiani body and the fusome mediate mitochondrial inheritance during *Drosophila* oogenesis. *Development* 130: 1579–1590
- DeLotto R, DeLotto Y, Steward R, Lippincott-Schwartz J (2007) Nucleocytoplasmic shuttling mediates the dynamic maintenance of nuclear dorsal levels during *Drosophila* embryogenesis. *Development* 134: 4233–4241
- Dietzl G, Chen D, Schnorrer F, Su K-C, Barinova Y, Fellner M, Gasser B, Kinsey K, Oettel S, Scheiblaue S et al (2007) A genome-wide transgenic RNAi library for conditional gene inactivation in *Drosophila*. *Nature* 448: 151–156
- Dong W, Dobler R, Dowling DK, Moussian B (2019) The cuticle inward barrier in *Drosophila melanogaster* is shaped by mitochondrial and nuclear genotypes and a sex-specific effect of diet. *PeerJ* 7: e7802
- Fortini P, Ferretti C, Iorio E, Cagnin M, Garribba L, Pietraforte D, Falchi M, Pascucci B, Baccharini S, Morani F et al (2016) The fine tuning of metabolism, autophagy and differentiation during in vitro myogenesis. *Cell Death Dis* 7: e2168
- Fujita N, Huang W, Lin T-H, Groulx J-F, Jean S, Nguyen J, Kuchitsu Y, Koyama-Honda I, Mizushima N, Fukuda M et al (2017) Genetic screen in *Drosophila* muscle identifies autophagy-mediated T-tubule remodeling and a Rab2 role in autophagy. *Elife* 6: e23367
- Galko MJ, Krasnow MA (2004) Cellular and genetic analysis of wound healing in *Drosophila* larvae. *PLoS Biol* 2: E239
- Gangishetti U, Veerkamp J, Bezdán D, Schwarz H, Lohmann I, Moussian B (2012) The transcription factor Grainy head and the steroid hormone ecdysone cooperate during differentiation of the skin of *Drosophila melanogaster*. *Insect Mol Biol* 21: 283–295

- Gonzalez-Estevez C, Felix DA, Aboobaker AA, Salo E (2007) Gtdap-1 promotes autophagy and is required for planarian remodeling during regeneration and starvation. *Proc Natl Acad Sci USA* 104: 13373–13378
- Hennig KM, Neufeld TP (2002) Inhibition of cellular growth and proliferation by dTOR overexpression in *Drosophila*. *Genesis* 34: 107–110
- Huang J, Zhou W, Dong W, Watson AM, Hong Y (2009) From the cover: directed, efficient, and versatile modifications of the *Drosophila* genome by genomic engineering. *Proc Natl Acad Sci USA* 106: 8284–8289
- Iyyathurai J, Decuypere JP, Leybaert L, D'Hondt C, Bultynck G (2016) Connexins: substrates and regulators of autophagy. *BMC Cell Biol* 17(Suppl 1): 20
- Jiang H, Patel PH, Kohlmaier A, Grenley MO, McEwen DG, Edgar BA (2009) Cytokine/jak/Stat signaling mediates regeneration and homeostasis in the *Drosophila* midgut. *Cell* 137: 1343–1355
- Kakanj P, Eming SA, Partridge L, Leptin M (2020) Long-term in vivo imaging of *Drosophila* larvae. *Nat Protoc* 15: 1158–1187
- Kakanj P, Moussian B, Gronke S, Bustos V, Eming SA, Partridge L, Leptin M (2016) Insulin and TOR signal in parallel through FOXO and S6K to promote epithelial wound healing. *Nat Commun* 7: 12972
- Kang J, Dong Z, Wang J, Chen G, Liu D (2019) Autophagy-related Djatg8 is required for remodeling in planarian *Dugesia japonica*. *Biol Open* 8: bio045013
- Kim JH, Jin P, Duan R, Chen EH (2015) Mechanisms of myoblast fusion during muscle development. *Curr Opin Genet Dev* 32: 162–170
- Kiss V, Jipa A, Varga K, Takáts S, Maruzs T, Lőrincz P, Simon-Vecsei Z, Szikora S, Földi I, Bajusz C et al (2020) *Drosophila* Atg9 regulates the actin cytoskeleton via interactions with profilin and Ena. *Cell Death Differ* 27: 1677–1692
- Klionsky DJ, Abdel-Aziz AK, Abdelfatah S, Abdellatif M, Abdoli A, Abel S, Abeliovich H, Abildgaard MH, Abudu YP, Acevedo-Arozena A et al (2021) Guidelines for the use and interpretation of assays for monitoring autophagy (4th edition)(1). *Autophagy* 17: 1–382
- Kurotani K-I, Tabata R, Kawakatsu Y, Sugita R, Okayasu K, Tanoi K & Notaguchi M (2020) Autophagy is induced during plant grafting for wound healing. bioRxiv <https://doi.org/10.1101/2020.02.14.949453> [PREPRINT]
- Lee T, Luo L (1999) Mosaic analysis with a repressible cell marker for studies of gene function in neuronal morphogenesis. *Neuron* 22: 451–461
- Levine B, Kroemer G (2019) Biological functions of autophagy genes: a disease perspective. *Cell* 176: 11–42
- Losick VP, Fox DT, Spradling AC (2013) Polyploidization and cell fusion contribute to wound healing in the adult *Drosophila* epithelium. *Curr Biol* 23: 2224–2232
- Martin AC, Kaschube M, Wieschaus EF (2009) Pulsed contractions of an actin-myosin network drive apical constriction. *Nature* 457: 495–499
- McGuire SE, Le PT, Osborn AJ, Matsumoto K, Davis RL (2003) Spatiotemporal rescue of memory dysfunction in *Drosophila*. *Science* 302: 1765–1768
- Milde R, Ritter J, Tennent GA, Loesch A, Martinez FO, Gordon S, Pepys MB, Verschoor A, Helming L (2015) Multinucleated giant cells are specialized for complement-mediated phagocytosis and large target destruction. *Cell Rep* 13: 1937–1948
- Moein S, Adibi R, da Silva ML, Nardi NB, Gheisari Y (2020) Cancer regeneration: polyploid cells are the key drivers of tumor progression. *Biochim Biophys Acta Rev Cancer* 1874: 188408
- Morin X, Daneman R, Zavortink M, Chia W (2001) A protein trap strategy to detect GFP-tagged proteins expressed from their endogenous loci in *Drosophila*. *Proc Natl Acad Sci USA* 98: 15050–15055
- Moussian B, Schwarz H (2010) Preservation of plasma membrane ultrastructure in *Drosophila* embryos and larvae prepared by high-pressure freezing and freeze-substitution. *Dros Inf Serv* 93: 215
- Nehme NT, Liegeois S, Kele B, Giammarinaro P, Pradel E, Hoffmann JA, Ewbank JJ, Ferrandon D (2007) A model of bacterial intestinal infections in *Drosophila melanogaster*. *PLoS Pathog* 3: e173
- Oda H, Tsukita S (2001) Real-time imaging of cell-cell adherens junctions reveals that *Drosophila* mesoderm invagination begins with two phases of apical constriction of cells. *J Cell Sci* 114: 493–501
- Pandit SK, Westendorp B, de Bruin A (2013) Physiological significance of polyploidization in mammalian cells. *Trends Cell Biol* 23: 556–566
- Patel PH, Thapar N, Guo L, Martinez M, Maris J, Gau CL, Lengyel JA, Tamanoi F (2003) *Drosophila* Rheb GTPase is required for cell cycle progression and cell growth. *J Cell Sci* 116: 3601–3610
- Pavel M, Rubinsztein DC (2017) Mammalian autophagy and the plasma membrane. *FEBS J* 284: 672–679
- Perkins LA, Holderbaum L, Tao R, Hu Y, Sopko R, McCall K, Yang-Zhou D, Flockhart I, Binari R, Shim H-S et al (2015) The transgenic RNAi project at harvard medical school: resources and validation. *Genetics* 201: 843–852
- Petrovsky R, Krohne G, Grosshans J (2018) Overexpression of the lamina proteins Lamin and Kugelkern induces specific ultrastructural alterations in the morphology of the nuclear envelope of intestinal stem cells and enterocytes. *Eur J Cell Biol* 97: 102–113
- Pignoni F, Zipursky SL (1997) Induction of *Drosophila* eye development by decapentaplegic. *Development* 124: 271–278
- Polychronidou M, Grobhans J (2011) Determining nuclear shape: the role of farnesylated nuclear membrane proteins. *Nucleus* 2: 17–23
- Polychronidou M, Hellwig A, Grosshans J (2010) Farnesylated nuclear proteins Kugelkern and lamin Dm0 affect nuclear morphology by directly interacting with the nuclear membrane. *Mol Biol Cell* 21: 3409–3420
- Qiang L, Yang S, Cui YH, He YY (2020) Keratinocyte autophagy enables the activation of keratinocytes and fibroblasts and facilitates wound healing. *Autophagy* 17: 2128–2143
- Ravikumar B, Moreau K, Jahreiss L, Puri C, Rubinsztein DC (2010) Plasma membrane contributes to the formation of pre-autophagosomal structures. *Nat Cell Biol* 12: 747–757
- Redman CWG, Staff AC, Roberts JM (2020) Syncytiotrophoblast stress in preeclampsia: the convergence point for multiple pathways. *Am J Obstet Gynecol* 226: S907–S927
- Rera M, Clark RI, Walker DW (2012) Intestinal barrier dysfunction links metabolic and inflammatory markers of aging to death in *Drosophila*. *Proc Natl Acad Sci USA* 109: 21528–21533
- Riggi M, Kusmider B, Loewith R (2020) The flipside of the TOR coin - TORC2 and plasma membrane homeostasis at a glance. *J Cell Sci* 133: jcs242040
- Riggi M, Niewola-Staszewska K, Chiaruttini N, Colom A, Kusmider B, Mercier V, Soleimanpour S, Stahl M, Matile S, Roux A et al (2018) Decrease in plasma membrane tension triggers PtdIns(4,5)P2 phase separation to inactivate TORC2. *Nat Cell Biol* 20: 1043–1051
- Royou A, Sullivan W, Karess R (2002) Cortical recruitment of nonmuscle myosin II in early syncytial *Drosophila* embryos: its role in nuclear axial expansion and its regulation by Cdc2 activity. *J Cell Biol* 158: 127–137
- Saito S, Nakashima A (2013) Review: the role of autophagy in extravillous trophoblast function under hypoxia. *Placenta* 34(Suppl): S79–84
- Scaffidi P, Misteli T (2006) Lamin A-dependent nuclear defects in human aging. *Science* 312: 1059–1063
- Scherfer C, Han VC, Wang Y, Anderson AE, Gallo MJ (2013) Autophagy drives epidermal deterioration in a *Drosophila* model of tissue aging. *Aging* 5: 276–287

- Schuh M, Lehner CF, Heidmann S (2007) Incorporation of *Drosophila* CID/ CENP-A and CENP-C into centromeres during early embryonic anaphase. *Curr Biol* 17: 237–243
- Schwenzfeier CW (1991) Recurrent facial paralysis associated with bouts of otitis media. *Am J Otol* 12: 466–467
- Scott RC, Juhasz G, Neufeld TP (2007) Direct induction of autophagy by Atg1 inhibits cell growth and induces apoptotic cell death. *Curr Biol* 17: 1–11
- Scott RC, Schuldiner O, Neufeld TP (2004) Role and regulation of starvation-induced autophagy in the *Drosophila* fat body. *Dev Cell* 7: 167–178
- Shrivage BV, Hill JH, Powers CM, Wu L, Baehrecke EH (2013) Atg6 is required for multiple vesicle trafficking pathways and hematopoiesis in *Drosophila*. *Development* 140: 1321–1329
- Struhl G, Basler K (1993) Organizing activity of wingless protein in *Drosophila*. *Cell* 72: 527–540
- Sun J, Tower J (1999) FLP recombinase-mediated induction of Cu/Zn-superoxide dismutase transgene expression can extend the life span of adult *Drosophila melanogaster* flies. *Mol Cell Biol* 19: 216–228
- Sylakowski K, Wells A (2021) ECM-regulation of autophagy: the yin and the yang of autophagy during wound healing. *Matrix Biol* 100–101: 197–206
- Takats S, Nagy P, Varga A, Pircs K, Karpati M, Varga K, Kovacs AL, Hegedus K, Juhasz G (2013) Autophagosomal Syntaxin17-dependent lysosomal degradation maintains neuronal function in *Drosophila*. *J Cell Biol* 201: 531–539
- Tang HW, Wang YB, Wang SL, Wu MH, Lin SY, Chen GC (2011) Atg1-mediated myosin II activation regulates autophagosome formation during starvation-induced autophagy. *EMBO J* 30: 636–651
- Tapon N, Ito N, Dickson BJ, Treisman JE, Hariharan IK (2001) The *Drosophila* tuberous sclerosis complex gene homologs restrict cell growth and cell proliferation. *Cell* 105: 345–355
- Varga M, Sass M, Papp D, Takacs-Vellai K, Kobolak J, Dinnyes A, Klionsky DJ, Vellai T (2014) Autophagy is required for zebrafish caudal fin regeneration. *Cell Death Differ* 21: 547–556
- Wang D, He J, Huang B, Liu S, Zhu H, Xu T (2020) Emerging role of the Hippo pathway in autophagy. *Cell Death Dis* 11: 880
- Wang Y, Antunes M, Anderson AE, Kadmas JL, Jacinto A, Galko MJ (2015) Integrin adhesions suppress syncytium formation in the *Drosophila* larval epidermis. *Curr Biol* 25: 2215–2227
- Wen JK, Wang YT, Chan CC, Hsieh CW, Liao HM, Hung CC, Chen GC (2017) Atg9 antagonizes TOR signaling to regulate intestinal cell growth and epithelial homeostasis in *Drosophila*. *Elife* 6: e29338
- Worman HJ, Courvalin JC (2005) Nuclear envelope, nuclear lamina, and inherited disease. *Int Rev Cytol* 246: 231–279
- Xu J, Ma Y, Zhu X, Zhang J, Cheng Z, Wu W, Wang P (2020) Enhanced autophagy promotes the clearance of *Pseudomonas aeruginosa* in diabetic rats with wounds. *Ann Transl Med* 8: 1362
- Xu T, Nicolson S, Denton D, Kumar S (2015) Distinct requirements of Autophagy-related genes in programmed cell death. *Cell Death Differ* 22: 1792–1802



License: This is an open access article under the terms of the Creative Commons Attribution-NonCommercial-NoDerivs License, which permits use and distribution in any medium, provided the original work is properly cited, the use is non-commercial and no modifications or adaptations are made.